

**EXAMINATION OF AN ACOUSTIC DATA SOURCE  
AND PAYLOAD FOR THE AUDIMUS CUBESAT  
MISSION**

**EXAMEN D'UNE SOURCE DE DONNEES  
ACOUSTIQUES ET D'UNE CHARGE UTILE POUR  
LA MISSION CUBESAT AUDIMUS**

Thesis Submitted to the Division of Graduate Studies  
of the Royal Military College of Canada  
by

David J. Anderson, CD, BSc  
Major

In Partial Fulfillment of the Requirements for the Degree of  
Master of Science in Physics

November 2024

© This thesis may be used within the Department of National Defence  
but copyright for open publication remains the property of the author.

*For Brianna, Samantha, and Matthew*

## **Acknowledgements**

I would first like to extend my gratitude to my supervisors, Dr. Ron Vincent, Dr. Jennifer Shore, and Dr. Dan Shan whose guidance and mentorship has been integral to the success of this research and to my success and professional development as a researcher. I'd also like to thank Dr. L Sangalli and the rest of the Audimus team for their input and direction. Finally, I would like to thank my wife Theresa for her unwavering support in all my endeavours. None of this would have been possible without her.

## **Abstract**

Climate change is disproportionately affecting the Arctic, fueled by rapidly warming temperatures, the melting of sea ice is making the Canadian Arctic more navigable each year. With the Arctic becoming more accessible to foreign actors, along with changing geopolitical landscapes, Canada faces new security challenges in the region. Highlighted in its most recent defence policy update, Canada has an urgent need to establish greater presence and reach throughout its northern regions. To support this goal, the Royal Military College of Canada, sponsored by Defence Research and Development Canada, and in partnership with the Canadian Space Agency's CubeSats Initiative in Canada for STEM program, will launch the Audimus satellite in 2026. The Audimus satellite mission will demonstrate a technological relay system to enable the transfer of acoustic data from hydrophones strategically positioned within the Canadian Arctic Archipelago to a ground station located at RMC.

This thesis explores the design, development, and deployment, of an acoustic data source and payload for the Audimus mission. Operating in the harsh arctic environment presents unique challenges, therefore several locations for deployment of a hydrophone system, along with seasonal weather and ice dynamics are considered. Under ice acoustics and bathymetry impact the operation and deployment of the systems and several hydrophone systems are presented. Ionospheric conditions in the Arctic are more dynamic than at lower latitudes and a detailed analysis of the communication link between the hydrophone and satellite ensures successful data collection. This communication link ultimately drives satellite payload design, and the suitable systems for the mission are highlighted. The findings from the Audimus mission will contribute to the continued development of satellite-based acoustic monitoring systems, offering insights into their operational challenges and further applications in the Arctic.

## Résumé

Le changement climatique affecte l'Arctique de manière disproportionnée. Alimentée par le réchauffement rapide des températures, la fonte de la glace de mer rend l'Arctique canadien plus navigable d'année en année. L'Arctique devenant plus accessible aux acteurs étrangers et les paysages géopolitiques changeant, le Canada est confronté à de nouveaux défis en matière de sécurité dans la région. Comme le souligne la dernière mise à jour de sa politique de défense, le Canada a un besoin urgent d'accroître sa présence et sa portée dans les régions septentrionales. Pour atteindre cet objectif, le Collège militaire royal du Canada, parrainé par Recherche et développement pour la défense Canada et en partenariat avec l'Initiative CubeSats au Canada pour le programme STEM de l'Agence spatiale canadienne, lancera le satellite Audimus en 2026. La mission du satellite Audimus fera la démonstration d'un système de relais technologique permettant le transfert de données acoustiques à partir d'hydrophones stratégiquement positionnés dans l'archipel arctique canadien vers une station terrestre située au CMR.

Cette thèse explore la conception, le développement et le déploiement d'une source de données acoustiques et d'une charge utile pour la mission Audimus. Le fonctionnement dans l'environnement arctique difficile présente des défis uniques, c'est pourquoi plusieurs emplacements pour le déploiement d'un système d'hydrophone, ainsi que les conditions météorologiques saisonnières et la dynamique de la glace sont pris en compte. L'acoustique et la bathymétrie sous la glace ont un impact sur le fonctionnement et le déploiement des systèmes et plusieurs systèmes d'hydrophones sont présentés. Les conditions ionosphériques dans l'Arctique sont plus dynamiques qu'à des latitudes plus basses et une analyse détaillée de la liaison de communication entre l'hydrophone et le satellite garantit la réussite de la collecte des données. Ce lien de communication détermine en fin de compte la conception de la charge utile du satellite, et les systèmes adaptés à la mission sont mis en évidence. Les résultats de la mission Audimus contribueront au développement continu des systèmes de surveillance acoustique par satellite, en donnant un aperçu des défis opérationnels et des applications futures dans l'Arctique.

# Contents

Acknowledgements .....	iii
Abstract .....	iv
Résumé.....	v
List of Tables .....	viii
List of Figures .....	ix
List of Acronyms and Abbreviations.....	xi
1 Introduction.....	1
1.1 Climate Change in the Arctic .....	1
1.2 Canadian Arctic Sovereignty.....	2
1.3 Audimus Mission .....	3
1.4 Strategic Arctic Areas.....	5
1.5 Thesis outline .....	6
2 Lancaster Sound.....	8
2.1 Location and surrounding area .....	8
2.2 Seasonal weather .....	9
2.3 Ice Dynamics.....	10
2.4 Atmospheric.....	11
3 Underwater Acoustics and Hydrophones .....	14
3.1 Acoustic Theory .....	14
3.2 Acoustics in Lancaster Sound and the NWP.....	17
3.3 Acoustic Data Source .....	22
3.4 The Sonobuoy .....	24
3.5 Sonobuoy placement .....	27
4 Communications - Hydrophone to Audimus.....	29
4.1 Satellite Communications Theory .....	29
4.2 Atmospheric Effects.....	30
4.3 Link Budget.....	32
4.4 Additional Link Considerations .....	35
5 High Altitude Balloon Mission .....	38
5.1 Description of Mission .....	38

5.2	System Design.....	38
5.3	Data Collection.....	41
5.4	Data Analysis .....	42
6	Audimus Payload .....	45
6.1	Requirements.....	45
6.2	Receiver Systems .....	45
7	Audimus Operations.....	48
7.1	Communications Testing.....	48
7.2	Mission Operations .....	48
7.3	Mission Continuation .....	49
8	Conclusion.....	52
	Bibliography.....	54

## List of Tables

Table 4.1 Satellite received carrier power for sonobuoy transmission of 173.5 MHz .....	34
Table 4.2 Satellite received carrier power for sonobuoy transmission of 136.0 MHz .....	34
Table 4.3 Summary of calculated and required EbNo and SNR with link margin for all sonobuoys. $f = 173.5$ MHz. ....	35

# List of Figures

Figure 1.1: Average monthly Arctic sea ice extent from satellite observations of the Arctic, 1978 to 2023 [4]. Observations in September show yearly minimum extent. .... 1

Figure 1.2: Map of the Northwest Passage that transits through the Canadian Arctic Archipelago [9]. .... 2

Figure 1.3: Audimus Concept of Operations (adapted from [21]). .... 4

Figure 1.4: STK Software simulation of the Audimus Orbit with the planned Arctic hydrophone position and the RMC ground station location [23]. .... 5

Figure 1.5: Map of the strategic sites in the Canadian Arctic Archipelago highlighting names of key locations and passages [25]. The white dashed lines show surface currents while the brown dashed lines show deeper, warmer ocean currents. .... 6

Figure 2.1 Map of Lancaster Sound and surrounding islands [27]. .... 8

Figure 2.2 Surface currents in Lancaster Sound (adapted from [38]). Arrows show direction and strength with larger arrows indicating stronger current. Crosshatching indicates sea ice extent for August 2018. .... 10

Figure 2.3 Satellite imagery of an ice arch in Lancaster Sound, taken on 18 February 2019. Mobile ice pack flowing eastward into Baffin Bay is visible. Imagery collected from National Oceanic and Atmospheric Administration (NOAA) Comprehensive Large Array-data Stewardship System (CLASS) [41]. .... 11

Figure 2.4 Total Magnetic Field Intensity (nT) over the Arctic using the WMM [43]. Magnetic field strength shown by the red contours. .... 12

Figure 2.5 Observed and Predicted Solar Cycle Sunspot Number Progression [45]. .... 12

Figure 2.6 Auroral zone shown expanding with increasing geomagnetic activity (left to right) severity [47]. .... 13

Figure 3.1 Typical deep-water SVP showing characteristic layers (adapted from [54]). .... 15

Figure 3.2 Refracted and surface-reflected ray paths in an Arctic water structure (left) and SVP (right) (adapted from [55]). Ray paths are identified by the initial grazing angle with the horizontal, where grazing angle is given by  $\theta - 90^\circ$ . Limiting ray path and shadow zone are shown. .... 16

Figure 3.3 Reflected ray paths in an Arctic water structure (adapted from [55]). The limiting ray path with a grazing angle of  $16^\circ$  is shown with further angles increasing in  $2^\circ$  increments. .... 16

Figure 3.4 Example of a deep sound channel (right) with associated SVP (left) (adapted from [59]). .... 17

Figure 3.5 Typical ray path diagram and corresponding sound speed profile for sound propagation in the eastern Arctic [52]. .... 18

Figure 3.6 Seasonal Sound Speed Profiles for the Northwest Passage, with +/- standard deviation bounds shown as dotted lines [25]. Winter SVP shown on left and summer SVP on the right .... 18

Figure 3.7 Seabed topography through Lancaster Sound [65]. White lines indicate the location of ridges and grooves. Color scale indicates depth in m. .... 19

Figure 3.8 Noise level for various ship classes as a function of frequency compared to the Wales-Heitmeyer model [68]. .... 20

Figure 3.9 Ambient noise levels near Lancaster Sound between August 2018 and May 2019 [67]. Color scale indicates noise level in dB for a given frequency.....	21
Figure 3.10 Radiated sound power of a submarine propeller and hull as a function of frequency [69]. Radiated power is shown with and without a hydraulic vibration absorber called a resonance charger (RC).....	22
Figure 3.11 LCC-VLA Concept (adapted from [71]).....	23
Figure 3.12 Schematic of the BSRT0 [19]. .....	24
Figure 3.13: Sonobuoy Components [76]. .....	25
Figure 3.14 MATLAB model of a representative sonobuoy radiation pattern at 173.5 MHz [79]. Model uses a monopole whip antenna with an infinite ground plane. Output frequency of 173.5 MHz is upper bound of sonobuoy transmission range. ....	26
Figure 3.15 Geobuoy in Arctic ice [81].....	27
Figure 4.1 Doppler shift of sonobuoy frequency band 136.0 MHz to 173.5 MHz. Horizon-to-horizon overhead pass for 600 km orbit.....	37
Figure 5.1 Balloon relay system layout components and conceptual layout. ....	39
Figure 5.2 VHF relay balloon payload prior to final assembly. ....	39
Figure 5.3: Dual band VHF/UHF L shape dipole antenna. ....	40
Figure 5.4: 4NEC2 Software simulation of a radiation pattern for an L shape dipole Antenna [105]. ....	40
Figure 5.5: Ground station for the VHF relay balloon.....	41
Figure 5.6 Flight path of the VHF relay balloon.....	42
Figure 5.7 Audacity interface showing spectrum comparison of multiple recordings with baseline recording (top row). The vertical axis shows amplitude while the horizontal axis shows time....	43
Figure 5.8 Resultant spectrum plot of a single recording using the frequency analysis in Audacity. ....	43
Figure 5.9: Losses in VHF recording shown with increasing slant range. Linear trendline shows increasing slope. ....	44
Figure 6.1 TOTEM SDR with wideband transceiver [120]. ....	46
Figure 6.2 ISSSPACE deployable CubeSat Antenna System for 1U/3U CubeSats [121]. ....	47
Figure 7.1 Initial Audimus Concept of Operations [21].....	50
Figure 7.2 STK simulation of the proposed Walker Delta constellation with paired satellite planes. Strategic areas and potential ground stations are also indicated [22]. ....	50

## List of Acronyms and Abbreviations

ADS-B	Automatic Dependent Surveillance-Broadcast
AIS	Automatic Identification System
AIT	Assembly, Integration, and Testing
AOPV	Arctic Offshore and Patrol Vessel
ASW	Anti-Submarine Warfare
BER	Bit Error Rate
BSRTO	Barrow Strait Real Time Observatory
CAA	Canadian Arctic Archipelago
CAATEX	Coordinated Arctic Acoustic Thermometry Experiment
CAF	Canadian Armed Forces
CCG	Canadian Coast Guard
CHAIM	Canadian High Arctic Ionospheric Models
CHAIN	Canadian High Arctic Ionospheric Network
CLASS	Comprehensive Large Array-data Stewardship System
COTS	Commercial Off-The-Shelf
CREATE	Collaborative Research and Training Experience program
CSA	Canadian Space Agency
DFO	Department of Fisheries and Oceans Canada
DIFAR	Directional Frequency Analysis and Recording
DRDC	Defence Research and Development Canada
DSP	Digital Signal Processor
EIRP	Effective Isotropic Radiated Power
EM	Electromagnetic
ESP	Electrospray Propulsion
GMSK	Gaussian Minimum Shift Keying
GPS	Global Positioning System
HAM	Amateur Radio
HQP	Highly Qualified Personnel
ISM	International Space Mission
LCC	Low Cost and Low Complexity
LEO	Low Earth Orbit
NOAA	National Oceanic and Atmospheric Administration
NSDIC	National Snow and Ice Data Center
NSERC	Natural Sciences and Engineering Research Council of Canada
OBC	Onboard Computer
RCAF	Royal Canadian Air Force
RCN	Royal Canadian Navy
RF	Radio Frequency
RMC	Royal Military College of Canada
SDR	Software Defined Radio
SNR	Signal-to-noise ratio
SOFAR	Sound Fixing and Ranging Channel
STK	Systems Tool Kit

SVP	Sound Velocity Profile
UHF	Ultra High Frequency
UNCLOS	United Nations Convention on Law of the Sea
VHF	Very High Frequency
VLA	Vertical Line Array
WMM	World Magnetic Model
SSO	Sun-synchronous Orbit
APRS	Automatic Packet Reporting System

# 1 Introduction

## 1.1 Climate Change in the Arctic

Global climate change is disproportionately affecting the Arctic with the average annual air temperature rapidly rising over the last 50 years. From 1971 to 2017, the average annual air temperature in the Arctic increased at 2.4 times the average warming rate of the Northern Hemisphere [1]. Increased greenhouse gas emissions are the most significant driver of this change [2]. Rising amounts of carbon dioxide, methane, and other compounds in the atmosphere are trapping increasing amounts of heat, producing a greenhouse effect. The Arctic is more severely impacted by this effect. This observation is referred to as Arctic Amplification, a phenomenon where the surface air temperature in the Arctic warms at an amplified rate compared to the global average. It is a result of various feedback mechanisms unique to the Arctic including the loss of sea ice [3]. Declining sea ice coverage leads to increased absorption of solar radiation by the ocean, further warming the region and reducing ice coverage thereby fueling the feedback loop of Arctic amplification. As a result of this warming, the areal extent of sea ice coverage in the Arctic has declined steadily over the last 45 years. Satellite data from the National Snow and Ice Data Center (NSIDC) shows a downward linear trend of 12.2 percent per decade with a total reduction of over 3.45 million square kilometers of ice (Figure 1.1).

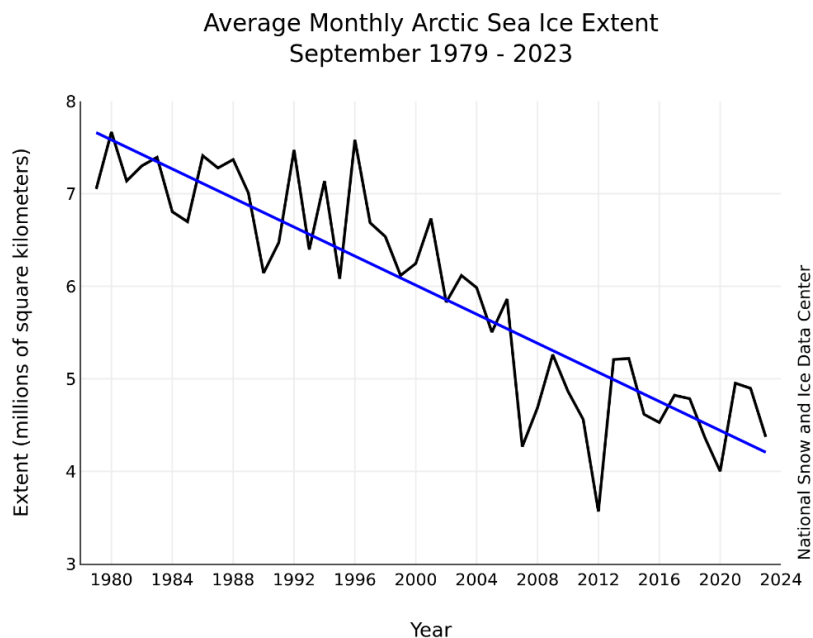


Figure 1.1: Average monthly Arctic sea ice extent from satellite observations of the Arctic, 1978 to 2023 [4]. Observations in September show yearly minimum extent.

The reduction in sea ice allows for increased activity in the Arctic such as shipping, resource extraction, tourism, and military operations. The global shipping community is particularly interested in northern shipping routes and shipping traffic in the Canadian Arctic has tripled between 1990 and 2015, with this linked directly to the reduction in sea ice cover [5], [6]. Of particular concern to Canadian Armed Forces (CAF) are challenges related to Canadian sovereignty due to the increased global interest in the Arctic with some competitors already attempting to take advantage by exploring Arctic waters and the sea floor [7].

## 1.2 Canadian Arctic Sovereignty

A more open and accessible Arctic invites increased use and presents challenges to Canada's Sovereignty. Canada considers the Canadian Arctic Archipelago, a grouping of 36 563 islands north of the Canadian mainland, a part of Canada's internal waters [8]. This area also includes the Northwest Passage, a sea route connecting the Atlantic and Pacific Oceans (Figure 1.2).



Figure 1.2: Map of the Northwest Passage that transits through the Canadian Arctic Archipelago [9].

Canada's claim is challenged by numerous countries including many allies: the United States, the European Union, Denmark, and Norway, which argue that the Northwest Passage is an international strait. A country's maritime boundaries are governed by the 1996 United Nations Convention on the Law of the Sea (UNCLOS), with the core difference between internal and international waters being the degree to which a state can control or prohibit the passage of foreign vessels [10]. Control of these waters is of great importance with respect to Canadian sovereignty. In a newly released defence policy update, the Canadian government identified asserting sovereignty in the Arctic and northern regions as a critically important task [7]. For a country to exert its sovereignty it

requires a persistent presence, the ability to monitor the area, and if necessary the ability to enforce its claim [11]. The indigenous population that calls the Arctic home, provides the presence required; however, in the areas of surveillance and enforcement Canada is lacking [12]. The Canadian Armed forces maintain a year-round presence of approximately 2000 personnel across Arctic locations. This is insufficient for an area encompassing more than 40% of Canada's land mass and 75% of its coastlines [13], [14]. Previous plans to procure nuclear submarines capable of extended transits under the Arctic ice and heavy icebreakers capable of patrolling the Arctic throughout the year were outlined in the 1987 Defence Policy: Challenge and Commitment [15]. These plans were never implemented and eventually replaced by the Royal Canadian Navy's (RCN) new Harry DeWolf class Arctic and Offshore Patrol Vessels (AOPV) [15]. Due to its multi-role design, its use for Arctic monitoring is limited. It is not capable of year round transit through heavy multi-year ice, has limited anti-ship armament, and no submarine detection capabilities [16], [17].

Canada also uses satellite technology to monitor traffic, Arctic sea ice extent and weather patterns [18]. However, these satellite systems, like the AOPV, lack the capability for sub-surface monitoring. There are few systems dedicated to under-ice acoustic monitoring of the Arctic. While the Barrow Strait Real Time Observatory (BSRTO) located in the Northwest Passage has demonstrated a capability for year-round operation, the acoustic data provided is limited to just two minutes of data per day, insufficient for monitoring of vessel traffic [19], [20]. To address these gaps in Arctic monitoring, the Canadian Government is making significant investments in underwater acoustic monitoring systems along with space-based surveillance and communication platforms. Planned funding over the next five years totals 51 million dollars for satellite systems and communications, 23 million for an Arctic satellite ground station, and 17 million for maritime sensors [7]. With the Arctic landscape rapidly changing, Canada's ability to monitor the Arctic must be improved. This is the driving force for the Audimus CubeSat mission.

### **1.3 Audimus Mission**

The Audimus mission is a 3U CubeSat being developed by the Royal Military College of Canada (RMC) in partnership with Defence Research and Development Canada (DRDC) and the Canadian Space Agency (CSA) [21]. The Audimus CubeSat will collect data from hydrophones located in the Canadian Arctic Archipelago, and subsequently relay the data to a ground station at RMC (Figure 1.3). This mission is intended to be the technological demonstration for a future satellite constellation project that would provide continuous coverage of target areas throughout the Canadian Arctic. The full satellite constellation was proposed by a previous RMC graduate student and is based upon their research [22]. Hydrophone data transmission will be in the very high frequency (VHF) range, data will be stored on the satellite and later forwarded to the RMC ground station via an ultra high frequency (UHF) downlink.

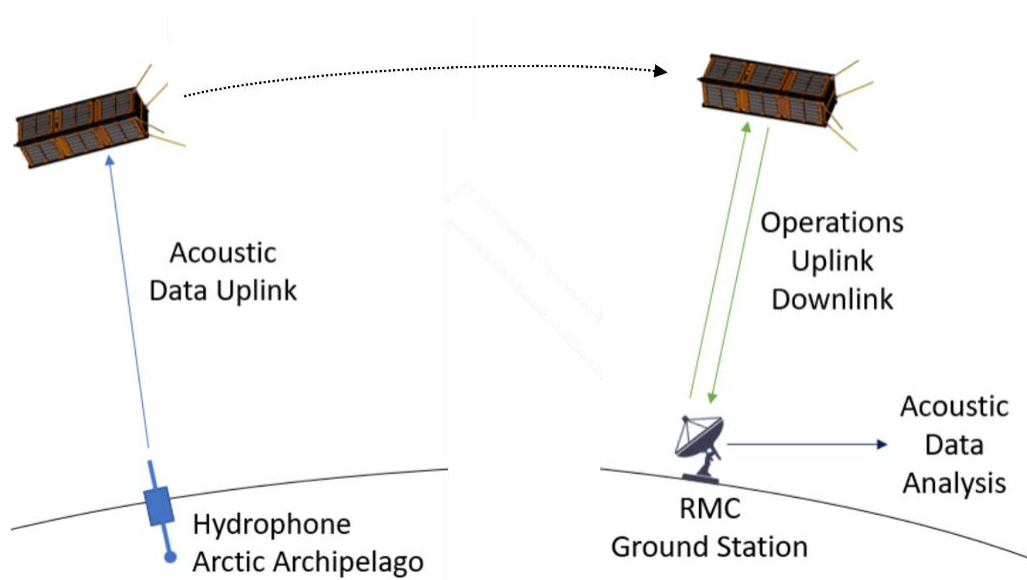


Figure 1.3: Audimus Concept of Operations (adapted from [21]).

The Audimus mission has four objectives. The first objective is to demonstrate a technological relay system that enables the transfer of data from hydrophones strategically positioned within the polar archipelagos of Canada and the ground station located at RMC. This objective holds significant importance from both scientific and strategic perspectives and is the focus of this thesis. The acoustic information collected by Audimus can be used to monitor both marine vessel traffic while also providing oceanic data for the study of ice dynamics and sea life. The second objective is to incorporate and test an Electrospray Propulsion (ESP) system developed at RMC. The aim of the ESP test is to prove the technology in orbit and if successful could later be used to assist in maintaining Audimus orbit or aid in de-orbiting. The third objective is to increase awareness and expertise in amateur radio while developing the amateur radio community at RMC. The final objective is to promote the education and training of highly qualified personnel (HQP) in the various sectors related to satellite missions.

Audimus is scheduled for launch in early 2026 and will be inserted into a sun-synchronous orbit (SSO), which as a polar orbit will allow for Arctic monitoring. While the exact orbital parameters will not be known until a launch contract is brokered by CSA, an orbital altitude between 550 and 600 km is expected. Computer simulations using software tool kit (STK) of the planned orbit show approximately fourteen accesses over the target area per day (Figure 1.4). The target area for monitoring has been chosen based on its strategic and scientific significance.

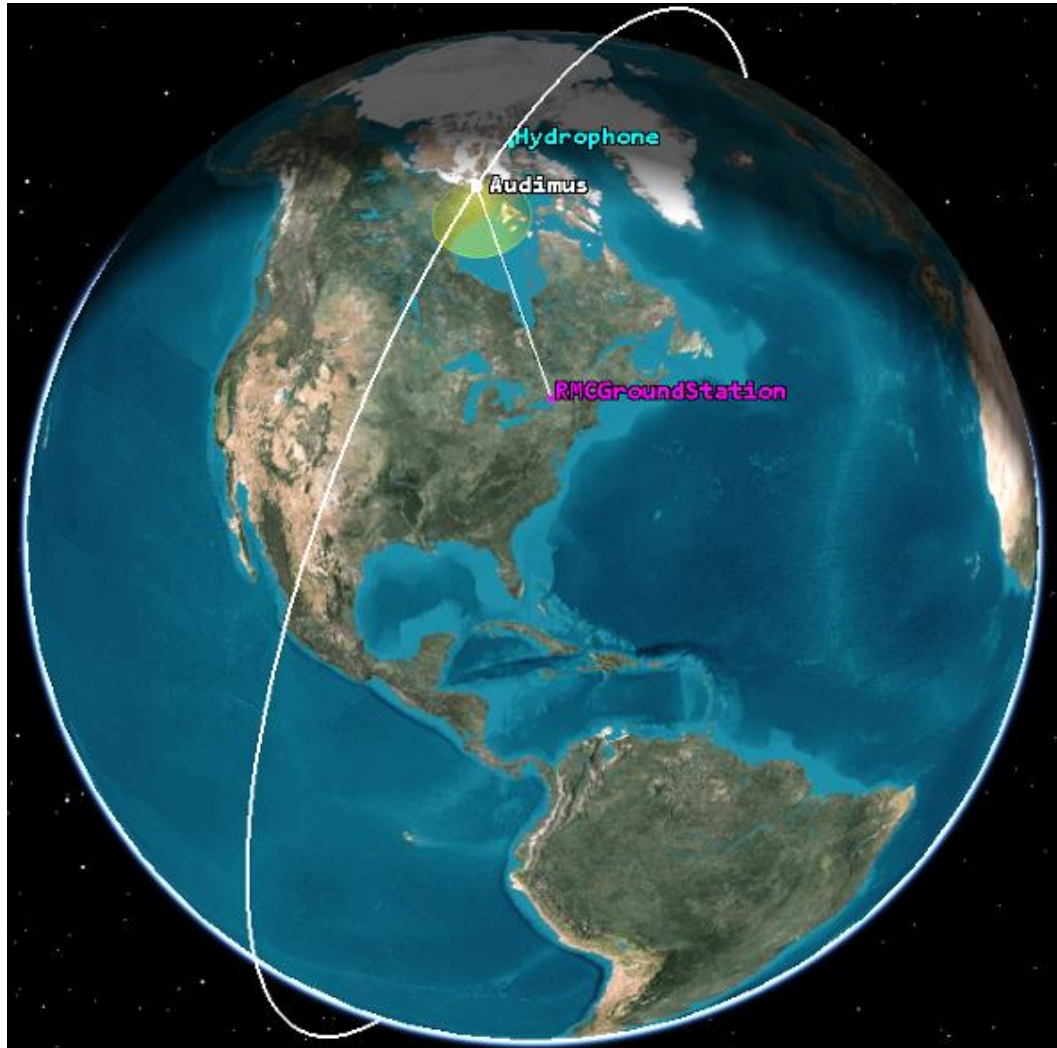


Figure 1.4: STK Software simulation of the Audimus Orbit with the planned Arctic hydrophone position and the RMC ground station location [23].

#### 1.4 Strategic Arctic Areas

Previous assessments conducted by DRDC identified five areas in the Canadian Arctic of strategic and acoustic importance (Figure 1.5). Sites A and B, located in the Canadian Basin and Beaufort Sea respectively, make up the western region of the Canadian Arctic Archipelago. Conditions at these sites consist of year-round ice coverage and deep acoustic sound channels [24]. Sites C and D encompass the eastern Northwest Passage. This area is generally ice covered 9 to 10 months of the year with strong tidal currents producing a mobile ice pack [25]. Site E in the Davis Strait has a strong seasonal cycle with open water conditions in the summer. Lancaster Sound, located between areas C and D was chosen as the hydrophone deployment site for the Audimus Mission.

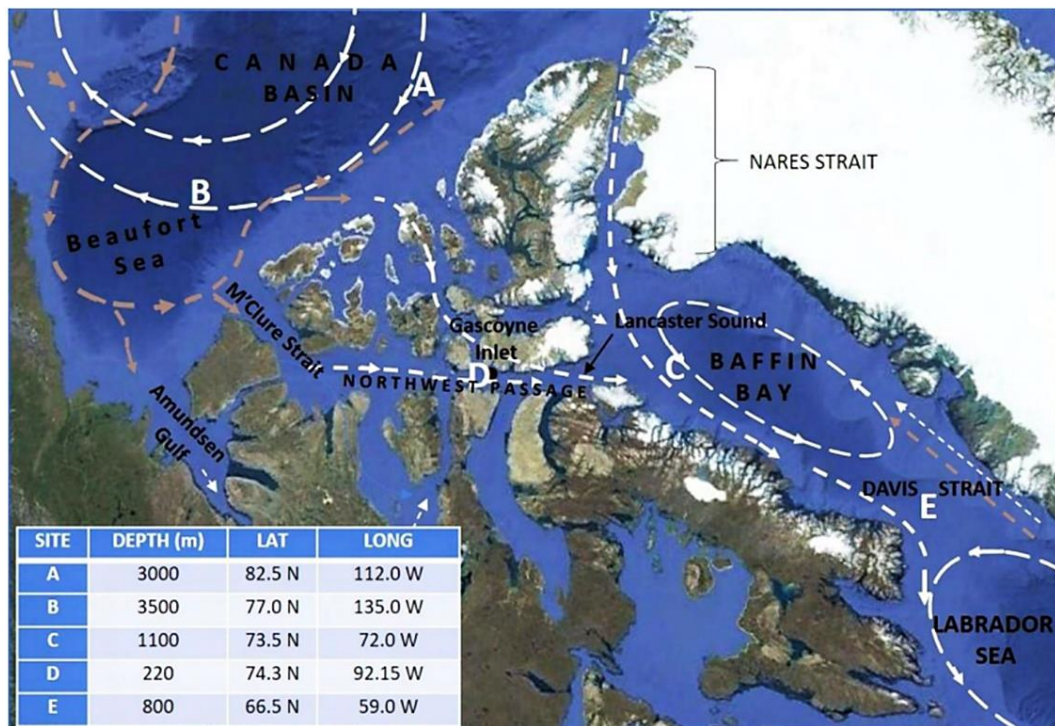


Figure 1.5: Map of the strategic sites in the Canadian Arctic Archipelago highlighting names of key locations and passages [25]. The white dashed lines show surface currents while the brown dashed lines show deeper, warmer ocean currents.

From a strategic perspective, Lancaster Sound marks the eastern entrance of the Northwest Passage. Any marine traffic wishing to transit the Arctic must pass through Lancaster Sound making it an excellent location for acoustic monitoring. Lancaster Sound is also an important habitat for marine life and acoustic data from this area will play a crucial role in conservation research of an environmentally sensitive area [26].

## 1.5 Thesis outline

Surveillance and reconnaissance of the Arctic are critical to identifying potential threats to Canadian security and sovereignty; however, Canada lacks a capable Arctic monitoring system. This thesis explores a proof-of-concept system using a nano satellite to relay acoustic data as a future Arctic surveillance system. The objective of this thesis is to provide an examination of an acoustic data source and related payload for the Audimus CubeSat mission. This mission will give RMC students hands-on experience with satellite design, assembly, integration, and testing. Developing local expertise with in-orbit operations and acoustic data analysis and payload design will be critical to the success of Audimus.

Section 2 provides background information on Lancaster Sound and the surrounding area. The Arctic is a unique and harsh environment, thus seasonal weather, ice dynamics, and

atmospheric conditions are all considered. Section 3 discusses the fundamental principles of underwater acoustics and acoustic theory. Arctic environments and the specific bathymetry of Lancaster Sound are highlighted. The impact of these factors on hydrophone systems and the challenges of operating in Arctic conditions is presented. Section 4 provides an overview of general satellite communications theory and atmospheric effects on Radio Frequency (RF) propagation. A detailed analysis of the communication link between a sonobuoy and satellite then follows. Section 5 discusses a related experimental high altitude balloon mission I participated in. Mission objectives, design and construction, data collection, and analysis of the collected data are presented. Section 6 outlines the necessary requirements for the primary payload, surveys available options, and highlights suitable systems. Finally, Section 7 summarizes the testing and operational program Audimus will undergo, acoustic data management, and follow on missions and research.

## 2 Lancaster Sound

This section provides background on Lancaster Sound and the surrounding area, highlighting seasonal weather, ice dynamics, and atmospheric conditions unique to the area. Lancaster Sound is a deep, narrow channel that is strategically located for acoustic monitoring of the Canadian Arctic. The area experiences extreme temperature variations affected by Arctic sunlight patterns and seasonal atmospheric changes. Ice cover lasts up to ten months, breaking up in summer to form a mobile ice field with a polynya forming annually in early winter. The region is home to more pronounced ionospheric phenomenon, particularly during periods of high solar activity.

### 2.1 Location and surrounding area

Lancaster Sound is a strategic and ecologically important location in the Canadian Arctic Archipelago. It is situated between Devon Island to the north and Baffin Island to the south and forms the eastern entrance to the Northwest Passage (Figure 2.1). A thorough understanding of Lancaster Sound is required to facilitate optimal hydrophone deployment.



Figure 2.1 Map of Lancaster Sound and surrounding islands [27].

Lancaster Sound is a deep, narrow sea passage that connects Baffin Bay to the east with the Barrow Strait to the west. It is approximately 300 km long and varies in width from roughly 65 km near Somerset island to 90 km at the entrance to Baffin bay [28]. Lancaster Sound is recognized as one of the most biologically diverse regions in the Arctic and is home to a seasonal Polynya. Polynyas are areas of the Arctic that remain largely ice free when local conditions suggest they should be ice covered. Polynyas are critical habitats for marine life providing a vital feeding and wintering area ground for numerous marine species [29]. Its nutrient-rich waters support large populations of marine mammals such as Narwhals, Belugas, Bowhead whales and seals, while the surrounding areas provide crucial breeding grounds for seabirds [29], [30]. Lancaster Sound is part of the Tallurutiup Imanga National Marine Conservation Area, safeguarding the ecological importance of the region. Its boundaries were established in 2017 and cover approximately 108 000 km<sup>2</sup>, making it the largest marine conservation area in Canada [31]. The region around Lancaster Sound has limited infrastructure due to its remote environment and harsh conditions. The nearby communities of Arctic Bay and Pond Inlet are predominantly Inuit and located on northern Baffin Island. Research stations, such as the BSRTO in Gascoyne Inlet, are also present conducting scientific studies in the region [19]. Like the rest of the Arctic, Lancaster Sound is facing environmental challenges due to climate change. The melting of sea ice, changes in ocean temperature and salinity, and potential impacts from shipping pose risks to this rich Arctic ecosystem and the marine life that depends on it [29].

## **2.2 Seasonal weather**

Lancaster Sound experiences extreme seasonal variations in weather with stark differences between the summer period, June to August, and winter period, November to March. During summer months average air temperatures are between 0°C and 10°C while the winter temperatures range between -20°C and -30°C [32]. These temperature extremes are strongly influenced by the presence of sunlight in the Arctic circle with continuous darkness in the winter and sunlight in the summer [33]. Lancaster Sound has strong, persistent winds. They predominantly flow from the northwest with an average speed of 19.5 km/h but regularly increase to speeds greater than 52 km/h. In the summer months the area is influenced by lower pressure systems from the Atlantic causing a shift from a southerly direction. Atmospheric pressure also varies seasonally. In the winter, low pressure systems provide cold stable weather with limited precipitation averaging 8 mm per month. In the summer, lower pressure systems bring more variability with increased precipitation averaging 30 mm monthly [32].

Circulation through Lancaster Sound is characterized by a unique combination of Arctic outflow and Atlantic inflow. Cold water from the Arctic Ocean flows southeastward through the Parry Channel into Lancaster Sound, influencing ice formation and drift while warmer water from the Atlantic Ocean flows westward creating a counter current [34]. While the net flow is southeastward, this mixing with warmer, more saline waters from Baffin Bay contributes to a cross-channel flow at the entrance of Lancaster Sound [35]. Currents along the southern shore flow eastward at an approximate rate of 10 cm/s during winter months and 25 cm/s during the summer with similar flow rates observed at all

depths. Conversely along the northern shore the flow is westward at a much weaker 3 cm/s and variable with depth [36], [37]. Surface currents in Lancaster Sound are shown in Figure 2.2. This seasonal climate variability has a strong influence on the ice dynamics of the local area.

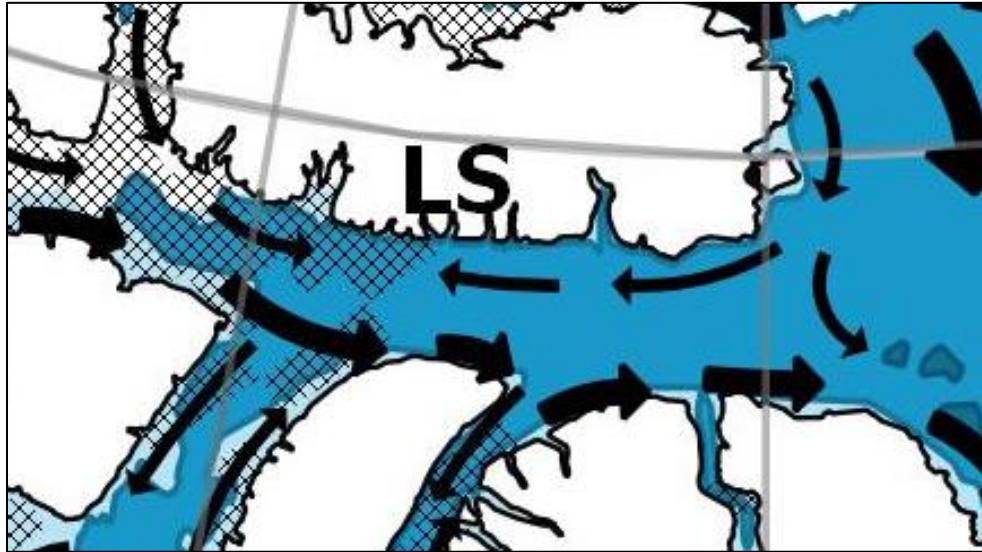


Figure 2.2 Surface currents in Lancaster Sound (adapted from [38]). Arrows show direction and strength with larger arrows indicating stronger current. Crosshatching indicates sea ice extent for August 2018.

### 2.3 Ice Dynamics

In Lancaster Sound, ice cover, both land-fast ice and pack ice, is common for approximately nine to ten months of the year. The ice pack typically breaks up in the summer months and along with strong currents, creates a mobile ice field [34]. As the ice flows eastward through the Lancaster Sound it forms an annual Polynya. There are a variety of factors that contribute to the formation of polynyas including seasonal variations in sensible and latent heat, surface winds, and ocean currents [39]. The Lancaster Sound polynya is just one of numerous polynyas that form seasonally in the Canadian Arctic Archipelago [39].

The Lancaster Sound polynya is formed when pack ice builds up in the strait and forms an ice arch. The ice arch location and date of formation is highly variable but has been observed since the advent of continuous satellite coverage in 1979 [40]. Formed in early winter, generally between December and April, the ice arch creates a border between the solid land-fast ice fastened to the shore and the mobile floe ice in open water (Figure 2.3). Once the ice arch is established in Lancaster Sound, newly formed ice is pushed eastward by winds and currents into Baffin Bay [40]. The freezing of Lancaster Sound occurs in an easterly direction along the path of the ice floe. Although the location of the ice arch formation is variable, the minimum observed distance measured from the northwestern tip of Bylot Island was 33 km [40].

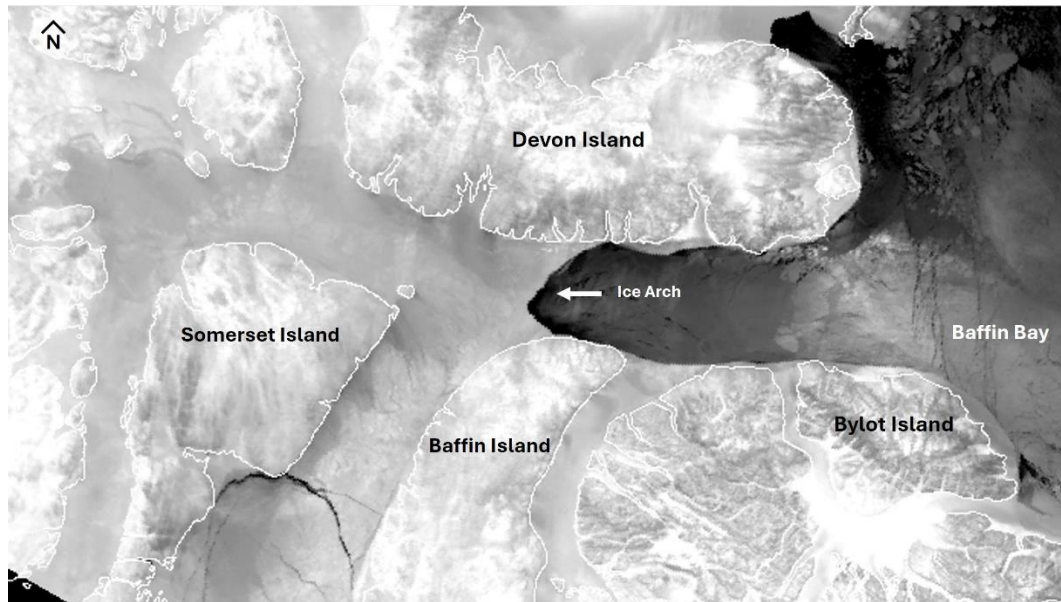


Figure 2.3 Satellite imagery of an ice arch in Lancaster Sound, taken on 18 February 2019. Mobile ice pack flowing eastward into Baffin Bay is visible. Imagery collected from National Oceanic and Atmospheric Administration (NOAA) Comprehensive Large Array-data Stewardship System (CLASS) [41].

## 2.4 Atmospherics

In addition to the environmental factors, there are some atmospheric properties unique to the Arctic. To ensure effective signal transmission to Audimus from Lancaster Sound these must be considered. The Earth's magnetic field, especially in regions near the poles like the Arctic, significantly influences radio frequency (RF) communications, affecting RF signal polarization. The Earth's Magnetic field strength in the Arctic is greater than that at lower latitudes, ranging between 50000 to 60000 nT, with values varying due to geomagnetic variations and local geological factors. Magnetic field lines vary around the North Magnetic Pole and the maximum field strength is offset with a maxima over northern Canada (Figure 2.4). Using the most recent World Magnetic Model (WMM), the five year average total field strength over Lancaster Sound is approximately 57200 nanotesla nT [42].

Ionospheric effects are also more pronounced in Arctic regions and will affect signal transmission, particularly during periods of high solar activity and solar proton events. This solar cycle is cyclical and predictable with the planned launch period for Audimus in 2026 is projected to be a period of increased solar activity (Figure 2.5). The predicted high for number of sunspots in January 2026 is approximately 122.5 [43]. the number sunspots indicative of the severity of geomagnetic activity.

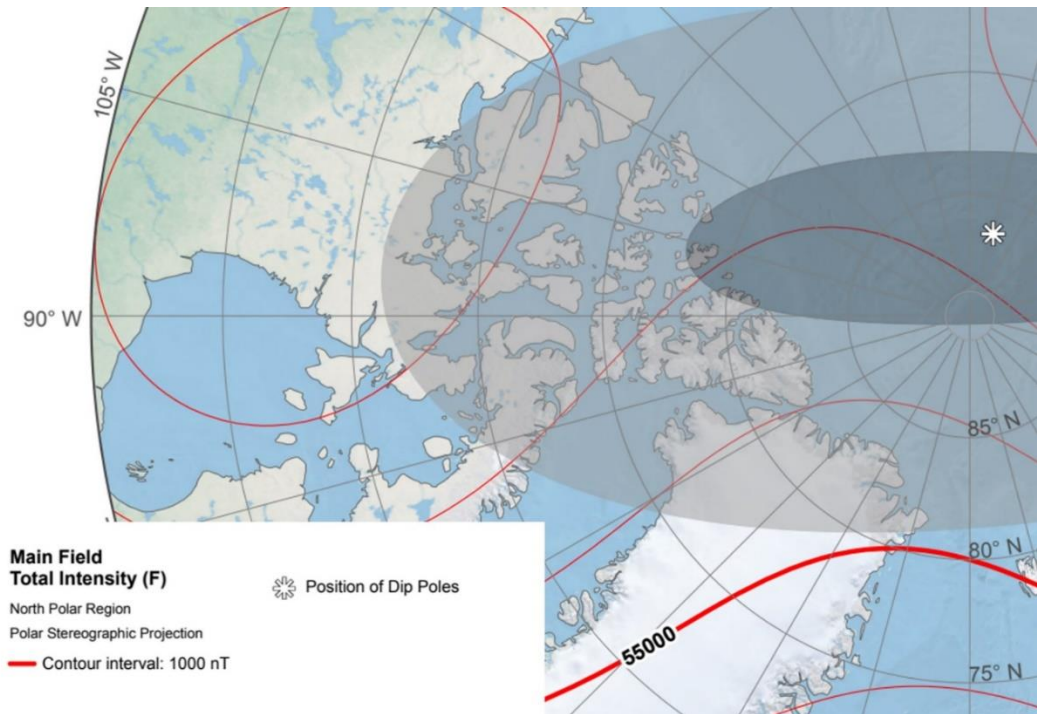


Figure 2.4 Total Magnetic Field Intensity (nT) over the Arctic using the WMM [44]. Magnetic field strength shown by the red contours.

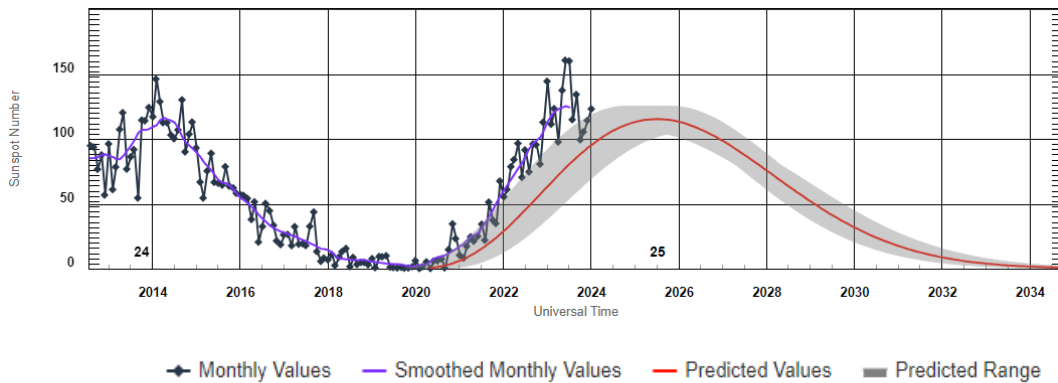


Figure 2.5 Observed and Predicted Solar Cycle Sunspot Number Progression [45].

The auroral and polar cap regions are unique zones in the Earth’s polar latitudes influenced by the interaction between the solar wind and the Earth’s magnetic field. The auroral zone is the region between 63° and 77° of latitude where the aurora is most frequently observed, while the polar cap zone is the region from 77° to 90° degrees latitude [46]. Auroral activity fluctuates based on solar activity, and the region expands toward the equator during geomagnetic storms (Figure 2.6) [47].

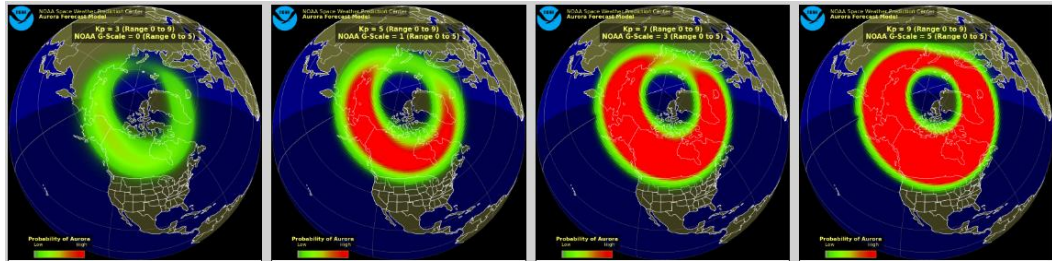


Figure 2.6 Auroral zone shown expanding with increasing geomagnetic activity (left to right) severity [47].

The ionosphere in Arctic regions is complex and subject to strong variability of electron density. This is directly coupled to the magnetic field and solar activity [48]. This solar activity negatively affects satellite communication by interacting with the earth's ionosphere, resulting in signal scintillation and fading along with ionospheric disturbances and delay. Prediction tools use ionospheric models, however, standard models become inaccurate at high latitudes. Since 2017 several Canadian High Arctic Ionospheric Models (CHAIM) have been created to overcome these deficiencies [49]. Near real-time ionospheric data is available from Canadian High Arctic Ionospheric Network (CHAIN) and has been used to validate CHAIM [48], [50]. These effects will be further explored in Section 4.

### 3 Underwater Acoustics and Hydrophones

This section discusses the fundamental principles of underwater acoustics and acoustic theory. The unique Arctic environment and specific bathymetry of Lancaster Sound dictate sound propagation in the region. Seasonal variations in sound speed and acoustic noise impact source detection. Arctic conditions dictate the design of and deployment of various hydrophone systems in an austere environment.

#### 3.1 Acoustic Theory

The propagation of sound through medium can be described by the acoustic wave equation. The standard form for a homogeneous medium where density is assumed to be constant is given by:

$$\Delta p - \frac{1}{c^2} \frac{\partial^2 p}{\partial t^2} = 0 \quad (3.1)$$

where  $p$  is the acoustic pressure (Pa),  $c$  is the speed of sound in the medium (m/s) and  $t$  is time (s) [51]. Note  $\Delta$  is the Laplacian operator  $\Delta = \frac{\partial^2}{\partial x^2} + \frac{\partial^2}{\partial y^2} + \frac{\partial^2}{\partial z^2}$ . For a harmonic wave with angular frequency  $\omega$  ( $\frac{rad}{s}$ ) ( $p \sim e^{-i\omega t}$ ) Equation (3.1) can be simplified to the time-independent Helmholtz equation:

$$\Delta p + k^2 p = 0 \quad (3.2)$$

where  $k = \omega/c$  is the wave number of sound ( $m^{-1}$ ) [51]. Solutions to the Helmholtz equation for specific geometrical assumptions and environments describe acoustic wave behavior [51], [52].

The speed of sound in seawater varies depending on temperature, salinity, and depth but can be approximated empirically with:

$$c = 1449.2 + 4.6T - 0.055T^2 + 0.00029T^3 + (1.34 - 0.01T)(s - 35) + 0.016z \quad (3.3)$$

where  $c$  is the speed of signal propagation through a medium, here  $c$  represents the speed of sound (m/s),  $T$  is the temperature ( $^{\circ}C$ ),  $S$  is salinity in parts per thousand, and  $z$  is the depth (m) [53]. Variations in temperature and salinity with water depth affect the propagation path of the sound wave. The speed of sound at various depths in the ocean is called the sound velocity profile (SVP). A typical SVP consists of four distinct regions. The surface layer is defined by mixing caused by wind, waves and surface temperature changes. This mixed layer is near-isothermal and is associated with the near-surface maximum sound speed [52]. This mixing often continues into the seasonal thermocline where the sound speed fluctuates with seasonal climate. In the main thermocline, temperature decreases rapidly with depth, leading to a pronounced decrease in sound

speed. This continues until reaching the deep sound channel, the point at which the sound speed reaches a minimum and the deep isothermal layer begins. In the deep isothermal layer the temperature is constant and the sound speed increases with increasing pressure [52]. Figure 3.1 shows a typical deep water sound speed profile.

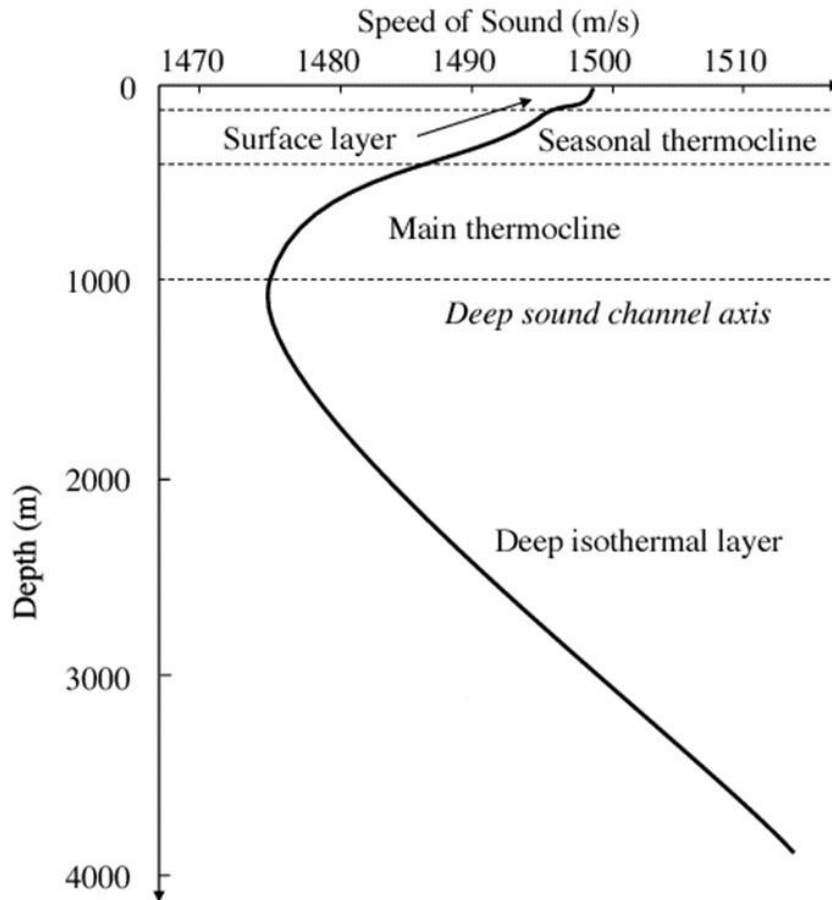


Figure 3.1 Typical deep-water SVP showing characteristic layers (adapted from [54]).

Using the SVP, the propagation path of sound waves through the ocean can be predicted. This is done by considering the water column as a combination of discrete horizontal layers and applying Snell's law:

$$\frac{\cos \theta_1}{c_1} = \frac{\cos \theta_2}{c_2} \quad (3.4)$$

where  $\theta_1$  is the angle between the incident sound ray and horizontal boundary,  $\theta_2$  is the angle between the refracted sound ray and the horizontal boundary, and  $c_1$  and  $c_2$  are sound speeds in their respective layers [55]. This relationship shows a refraction of the sound ray toward regions of lower speed. The ray path is dependent on the sound speed structure and the initial conditions at the source. For a constant positive gradient, typical for Arctic

waters, sound waves will bend upward. Upon reaching the surface the rays will be reflected downwards with a slight loss of energy. The ray that just grazes the bottom is called the limiting ray path. The shadow zone is just beyond this ray path and no direct path can reach that zone. Figure 3.2 shows the Arctic case.

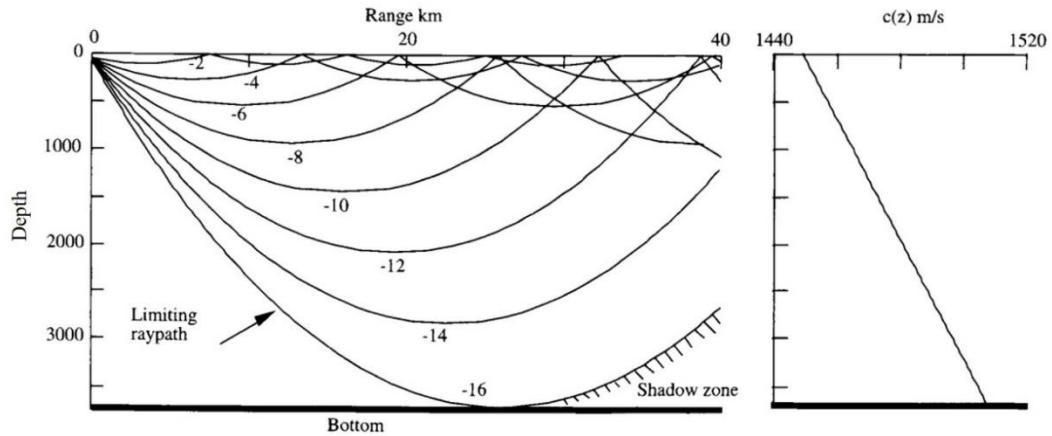


Figure 3.2 Refracted and surface-reflected ray paths in an Arctic water structure (left) and SVP (right) (adapted from [55]). Ray paths are identified by the initial grazing angle with the horizontal, where grazing angle is given by  $\theta - 90^\circ$ . Limiting ray path and shadow zone are shown.

Steeper ray paths, those beyond the limiting ray path will reflect from both the bottom and surface. This reflection will allow ray paths with at least two bottom bounces to penetrate the shadow zone, however this energy is attenuated exponentially [55]. Figure 3.3 shows the reflected ray paths.

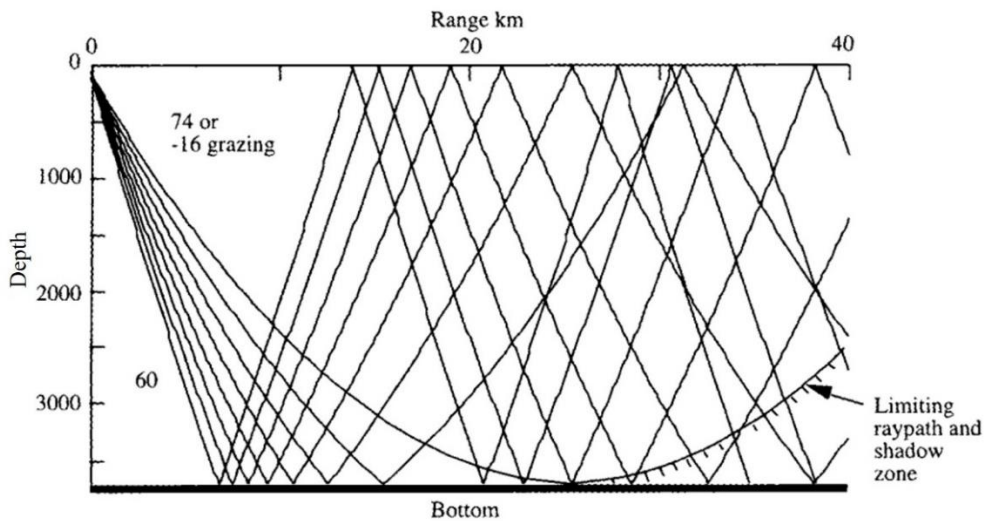


Figure 3.3 Reflected ray paths in an Arctic water structure (adapted from [55]). The limiting ray path with a grazing angle of  $16^\circ$  is shown with further angles increasing in  $2^\circ$  increments.

The deep sound channel, also known as the sound fixing and ranging (SOFAR) channel, allows for sound propagation over long ranges. It occurs at layers where the sound speed is at a minimum and can approach the surface in polar regions [56]. The sound waves are trapped between two boundaries of maximum sound speed (Figure 3.4). This focusing effect avoids the losses resultant from bottom and surface reflections. Sounds waves in the channel can travel up to thousands of kilometres before being attenuated [57].

Convergence zones are another type of ray path where the sound rays refract upward along similar paths converging at a specific location. This results in higher sounds levels due to focusing of the sound waves over long distances [55]. Convergence zones require strong upward sound speed profiles and deep water so that the sound waves do reflect off the sea floor or ice [52], [58]. This makes the occurrence of convergence zones in arctic waters unlikely.

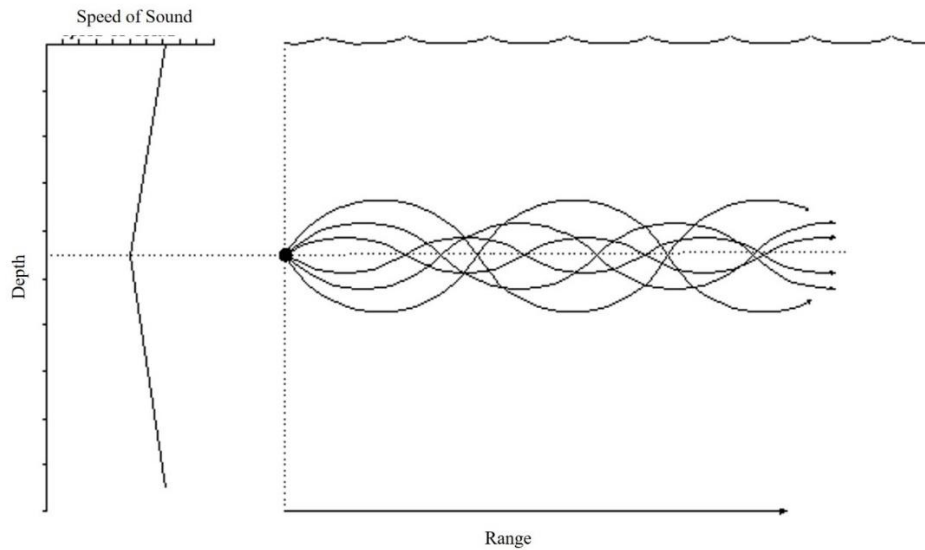


Figure 3.4 Example of a deep sound channel (right) with associated SVP (left) (adapted from [59]).

### 3.2 Acoustics in Lancaster Sound and the NWP

Sound propagation in Arctic environments is different than in temperate ones. In mid-latitude environments, temperature and salinity play larger roles than in polar regions where water columns are more uniform [60]. The Arctic features colder and less saline water producing a predominantly positive gradient sound speed profile, where sound speed increases with depth. This causes a continuously upward-refracting propagation that will repeatedly interact with ice covered surface waters (Figure 3.5).

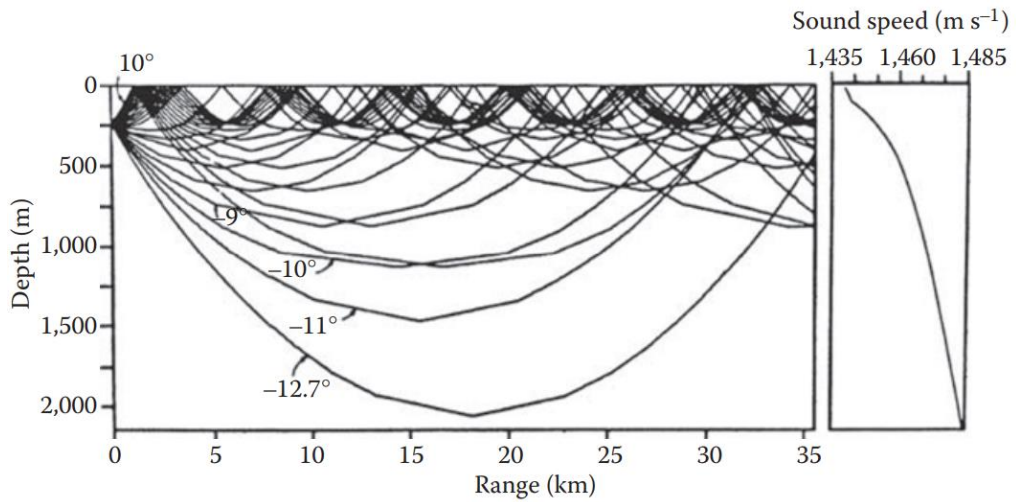


Figure 3.5 Typical ray path diagram and corresponding sound speed profile for sound propagation in the eastern Arctic [52].

The ice acts as an acoustic boundary, absorbing, reflecting and scattering the sound wave as it repeatedly interacts with the uneven surface under the sea ice. This causes sound propagation to degrade rapidly with increasing frequency, and mainly lower frequencies are caught in the sound channel [61]. Attenuation rapidly increases for frequencies above 30 Hz and acts as a low pass filter [52]. Sound speed profiles representative of Lancaster Sound are shown in Figure 3.6.

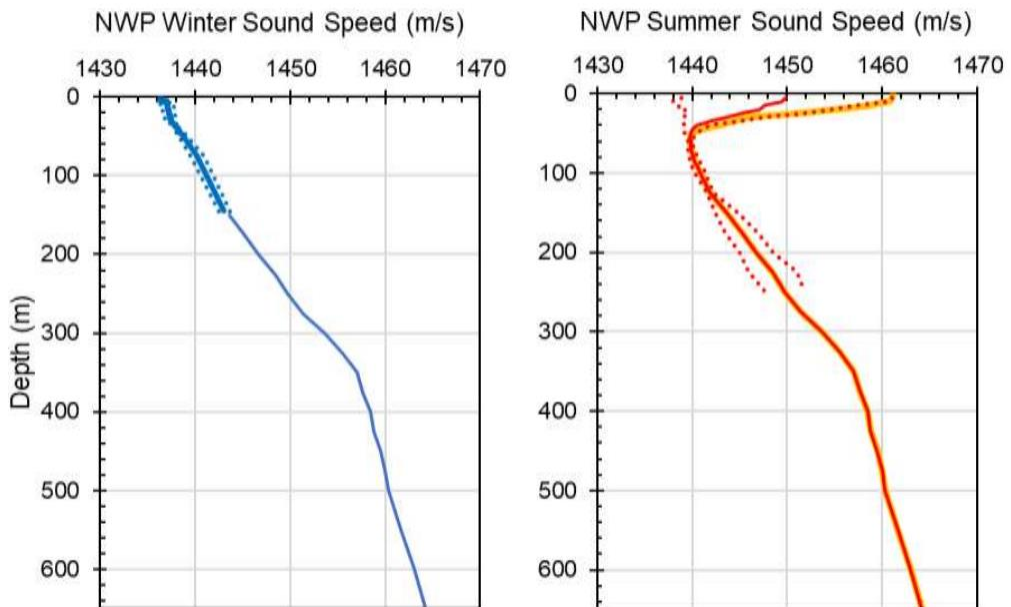


Figure 3.6 Seasonal Sound Speed Profiles for the Northwest Passage, with +/- standard deviation bounds shown as dotted lines [25]. Winter SVP shown on left and summer SVP on the right

Additional transmission loss is caused by the underwater topography and shallow-water conditions present in most of the Canadian Arctic Archipelago (CAA). As interactions with surface ice decreases the transmissible frequency, the lower frequencies then interact with the seabed further losing energy [62]. The resulting combined losses lead to a lower frequency bound of 5-10 Hz for long-range propagation [63]. The underwater topography of Lancaster Sound includes a mix of shallow shelves and deep troughs. Depths in Lancaster Sound range from 200 m to over 900 m. It is shallowest at the western end near Somerset Island and gradually slopes down towards the eastern entrance reaching a depth of more than 900m [64]. The sides of the channel are steeply sloped with a generally flat bottom consisting primarily of gravel and clay. There are irregularities in the bottom topography with channels, ridges and grooves attributed to retreating glacial ice sheets (Figure 3.7).

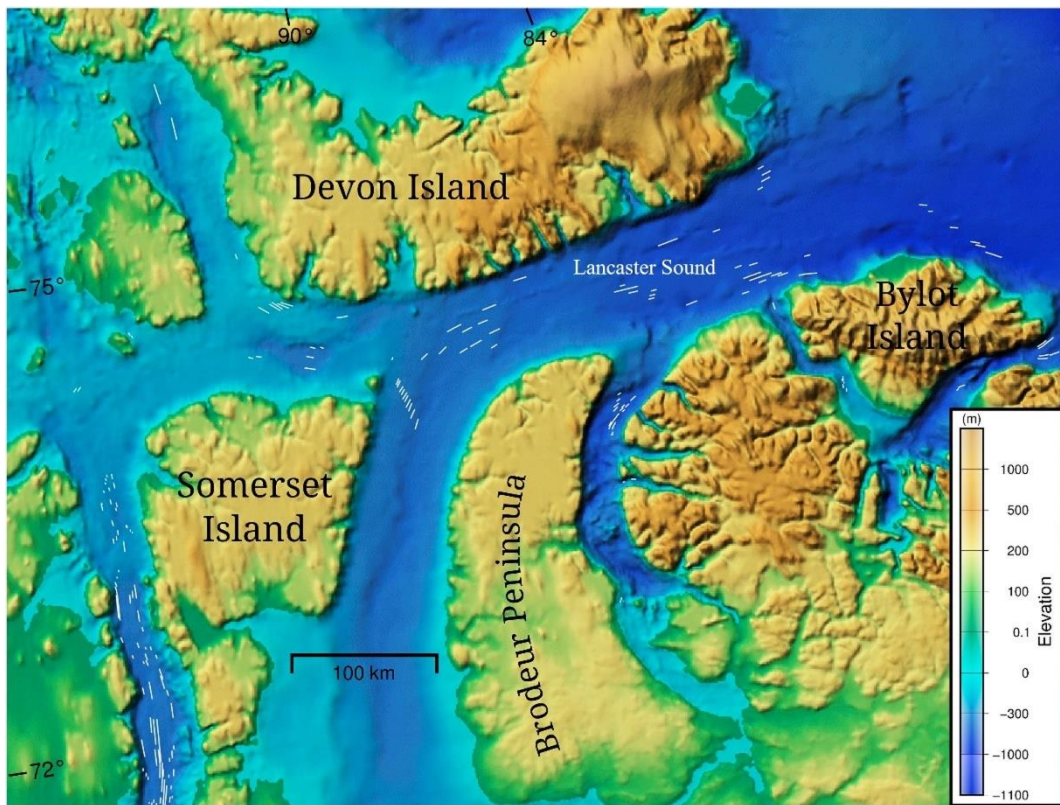


Figure 3.7 Seabed topography through Lancaster Sound [65]. White lines indicate the location of ridges and grooves. Color scale indicates depth in m.

There are generally less sources of ambient noise in Arctic environments like Lancaster Sound, resulting in less overall ambient noise than is found in lower latitude regions. These ambient noise sources vary depending on the time of year [66]. During the winter and spring, ice cracking and movement due to wind, current, and thermal stress are the primary source of noise. In the summer, this shifts with shipping noise and biological noise

becoming more prevalent [66]. Ice noise is generally categorized as a transient signal, or a short burst of energy deviating from a steady state. These transients occur across a wide frequency range of 50 to over 1000 Hz [67]. Biological noise predominantly comes from the Narwhals, Belugas, Bowhead whales, and seals which emit noise in the 50 Hz to 20 kHz range [67]. The majority of noise from shipping traffic is caused by propeller cavitation, but hull and mechanical vibrations also create noise [60]. According to the Wales-Heitmeyer model, ship noise ranges over a 30 to 1200 Hz frequency band, but propeller noise can be as low as 10 Hz [67], [68]. Figure 3.8, shows the acoustic signatures of various ships while a sample of ambient noise levels recorded by the BSRT0, near the western end of Lancaster Sound, is shown in Figure 3.9.

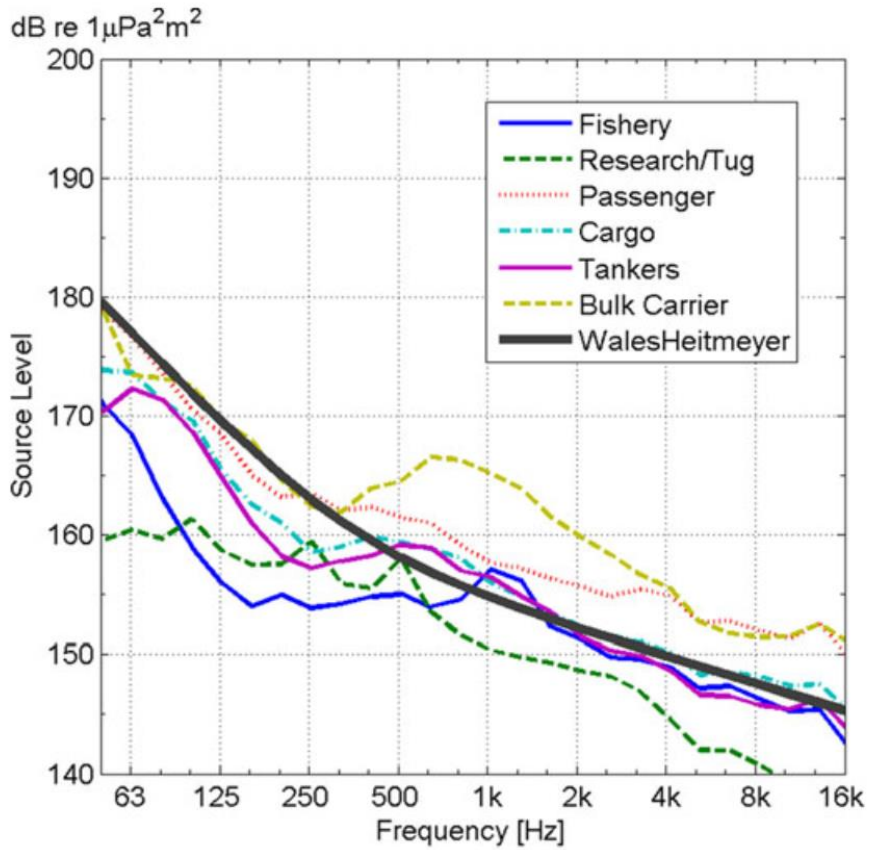


Figure 3.8 Noise level for various ship classes as a function of frequency compared to the Wales-Heitmeyer model [68].

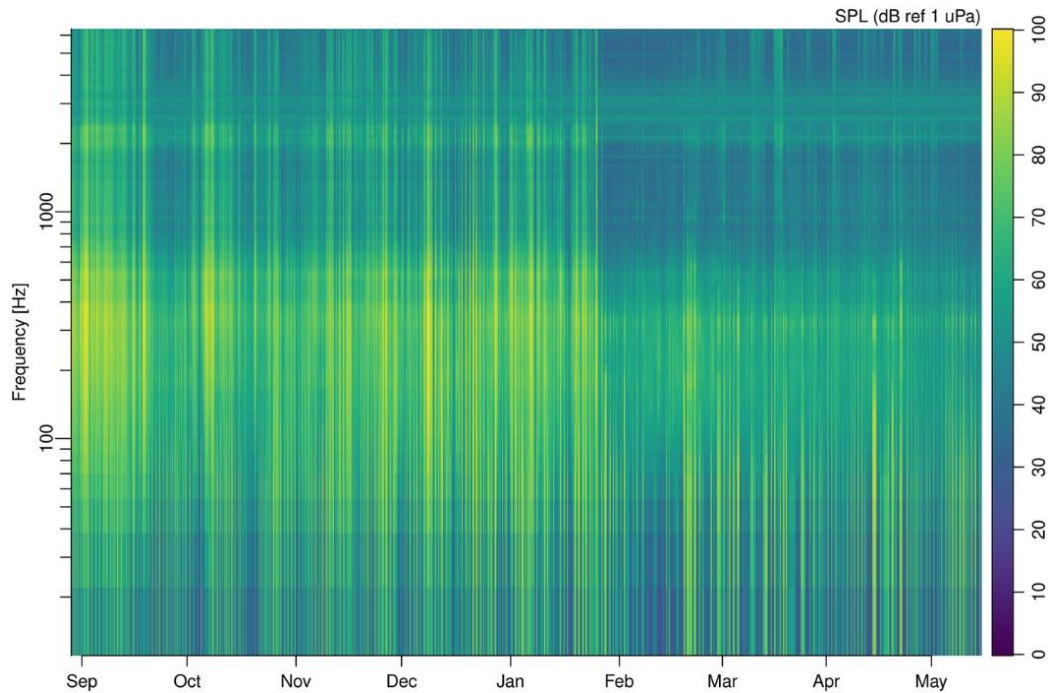


Figure 3.9 Ambient noise levels near Lancaster Sound between August 2018 and May 2019 [67]. Color scale indicates noise level in dB for a given frequency.

Noise generated by submarines is generally at frequencies below 300 Hz with frequencies below 80 Hz of primary interest [24]. Propeller noise can be as low as 5 Hz and is important for identifying the submarine class. The typical profile for noise generated by a submarine's propeller and hull is shown in Figure 3.10. The low frequency generated by propellers overlaps with the narrow frequency range of 5-10 Hz required for long range under ice propagation in Lancaster Sound suggesting long range detection of submarines is possible. The hydrophone system for Audimus should allow for detection in this low frequency range to optimize the chance of ship and submarine detection.

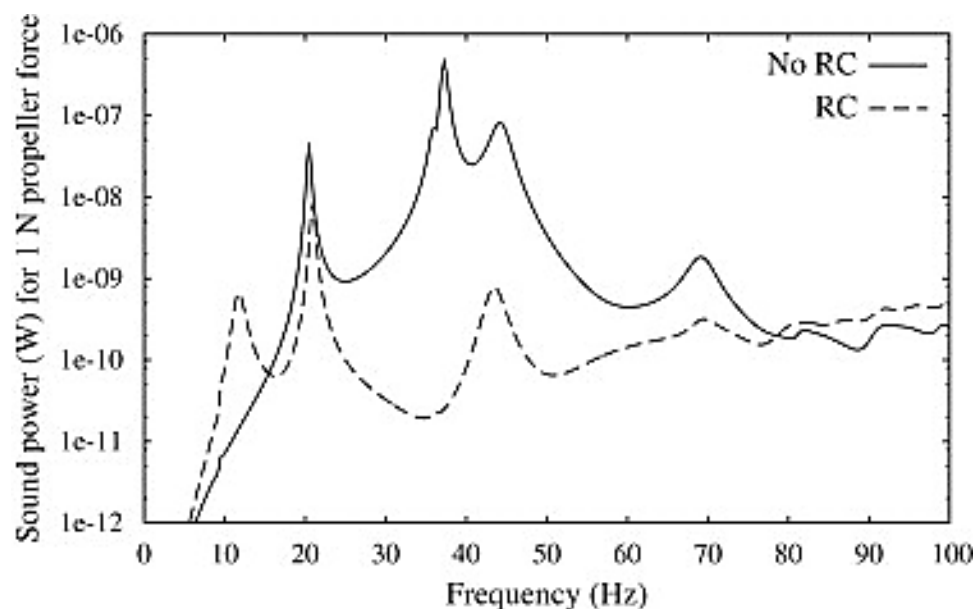


Figure 3.10 Radiated sound power of a submarine propeller and hull as a function of frequency [69]. Radiated power is shown with and without a hydraulic vibration absorber called a resonance charger (RC).

### 3.3 Acoustic Data Source

Two primary data sources are being developed to support the Audimus mission. First is a project for a low cost and low complexity vertical line array (LCC-VLA) of hydrophones for the Canadian Arctic environment while the second is a refurbishment of the existing BSRTO. Intended as a through-the-ice, extremely long-term sonobuoy, LCC-VLA is being developed by JASCO Applied Sciences for DRDC Atlantic as a remote monitoring system to bolster underwater surveillance in the Arctic and is an evolution of a previously outlined VLA drifter buoy [70]. The LCC-VLA includes a vertical hydrophone array, signal processing hardware, a GPS receiver, an Iridium radio, a hull for housing components and ice penetration, and a command center message parsing system (Figure 3.11) [71]. Operating in a 20 to 300 Hz band, it achieves signal detection through a combination of analog summation beamforming and a tailored digital signal processing algorithm. Hull design with a smaller, thicker design than the one used on the Coordinated Arctic Acoustic Thermometry Experiment (CAATEX) spar buoy [72]. The Seasonal Ice Mass Balance Buoy 3 provides a similar robustness with a modified version providing an alternative hull design [73]. The system's design emphasizes low power consumption, with a lightweight lithium battery pack that supports long-term operation of up to eight months, and a compact hull for easy deployment. Current challenges to include validating the system's robustness in Arctic conditions, optimizing stability during ice drift, and ensuring reliable real-time communication over extended periods. Initial open water testing is expected in 2025 with ice trials to follow.

### Mooring Diagram Ice Buoy Concept

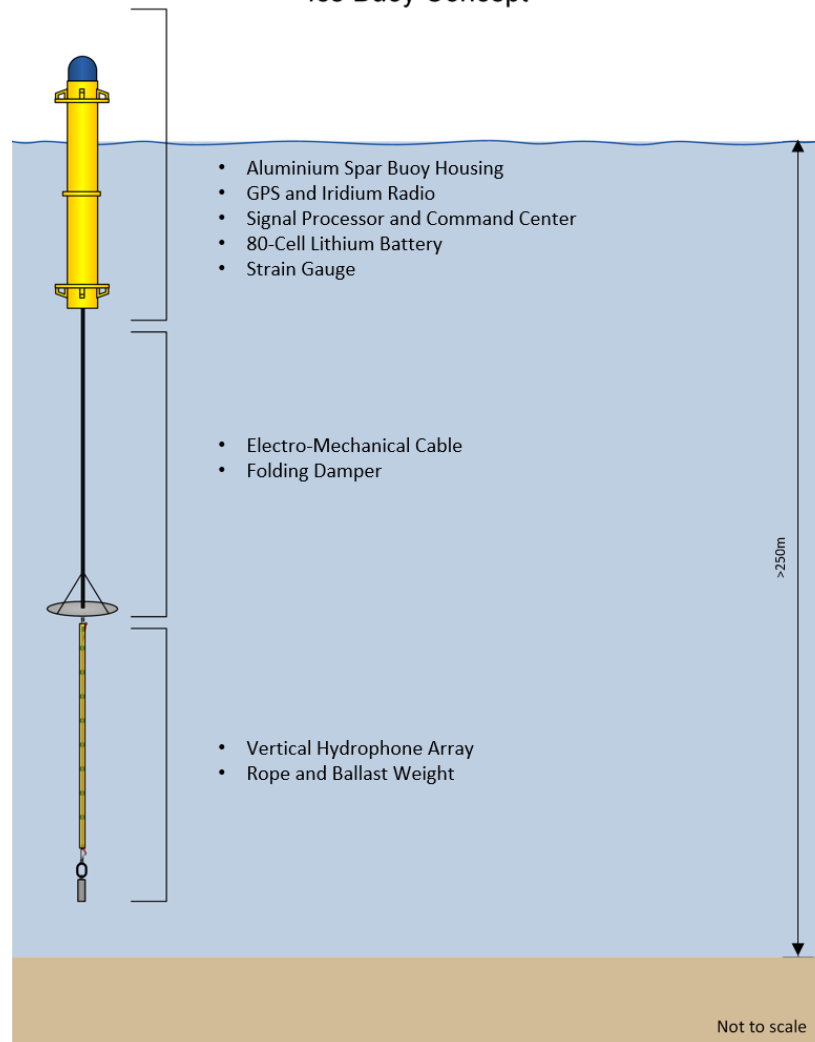


Figure 3.11 LCC-VLA Concept (adapted from [71]).

The BSRTO is a permanent monitoring system designed to collect and transmit environmental data from the Arctic region as part of a broader network of ocean observatories [20]. The observatory is equipped with a variety of sensors and instruments placed on the seafloor and throughout the surrounding water column. This includes a icListen hydrophone from Ocean Sonics that collects ambient sound measurements of the surrounding water column [74] daily. Sensor data is collected at an underwater data hub and then transmitted to a shore station for processing and transmission by the Iridium satellite network (Figure 3.12).

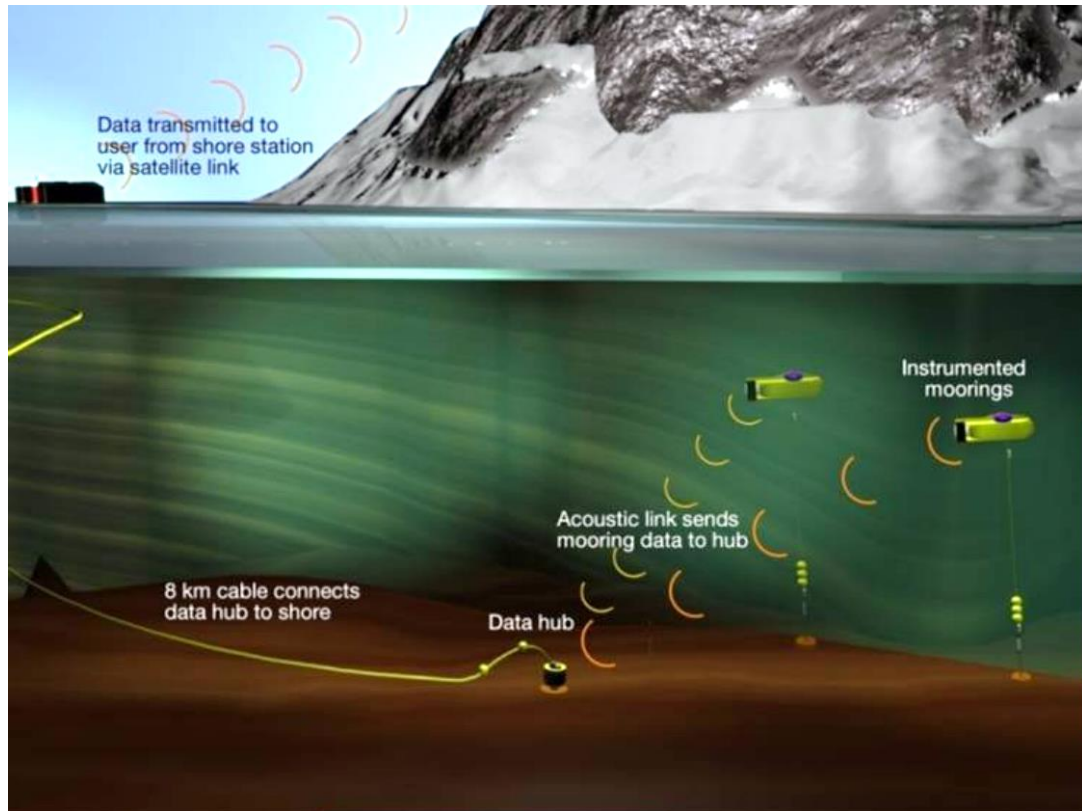


Figure 3.12 Schematic of the BSRTO [19].

Both systems are desirable as an alternative data source for the Audimus mission due to the greater longevity of the system when compared to a sonobuoy. In the case of the BSRTO this includes year-round data for the life of the Audimus mission. While these systems currently use Iridium, DRDC Atlantic has agreed to provide funding for the addition of a VHF transmitter. Although it is early in the development process, testing completion is planned for summer 2026, following the launch of Audimus.

### 3.4 The Sonobuoy

An additional data source for the Audimus mission will be a sonobuoy system. Sonobuoys will be used concurrently with the primary data sources and act as a backup in the event of development delays. Sonobuoys were first developed during World War II and are expendable, air-deployed systems, used primarily for anti-submarine warfare (ASW) [75]. Sonobuoys consist of a surface float containing a radio transmitter, antenna, electronics package, and saltwater-activated battery, along with an underwater component consisting of hydrophones and stabilizing equipment (Figure 3.13).

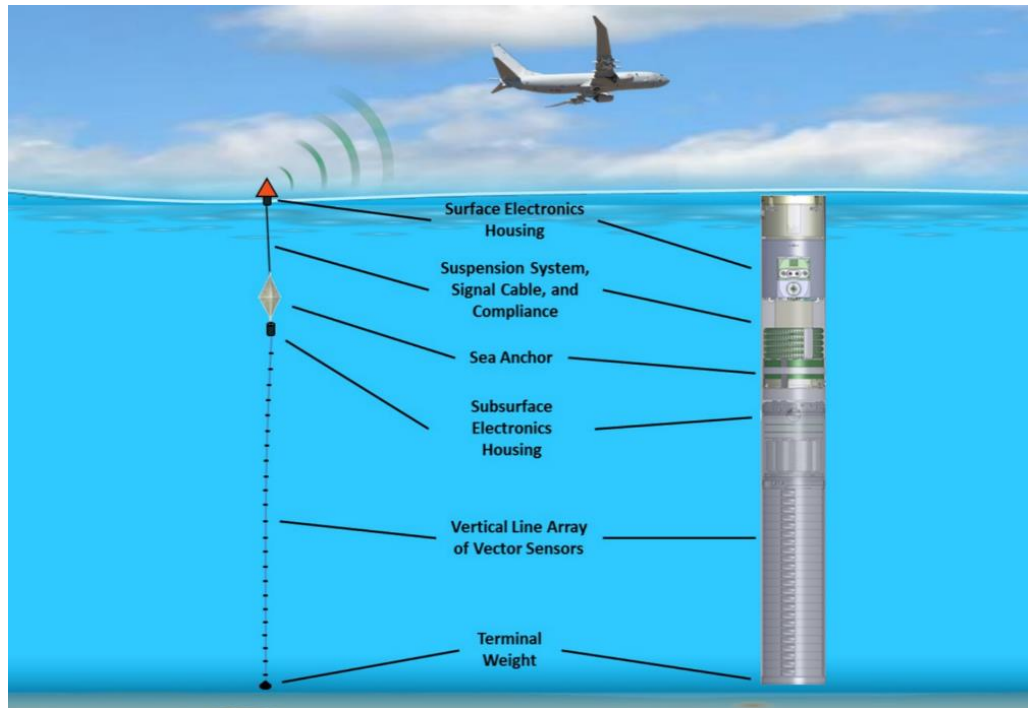


Figure 3.13: Sonobuoy Components [76].

Sonobuoys were chosen due to their flexibility and ability to be air-deployed to an austere environment like the Arctic. They are a proven system, regularly used by the Royal Canadian Air Force (RCAF) and Royal Canadian Navy (RCN) with the relayed data being of strategic importance. The downside to the use of the sonobuoys is their limited lifespan, a maximum of 8 hours once deployed, so additional hydrophone systems are still being considered. A challenge related to their limited life, is the coordination with RCAF or a company to ensure that the hydrophone gets deployed when required. However, alternative options exist, such as deployment by ships, with the RCN and Fisheries and Oceans Canada (DFO) being potential avenues. Waiting for an opportunity to join an existing tasking or submitting a request for employment to obtain Aurora support are also viable possibilities.

There are a multitude of sonobuoys commercially available and three from the CAF inventory are considered. The SSQ-53D Directional Frequency Analysis and Recording (DIFAR) sonobuoy, the SSQ-573 DIFAR sonobuoy, and Geobuoys. The SSQ-53D DIFAR sonobuoy is a proven system that provides directional and omnidirectional acoustic data. The hydrophones operate over a wide acoustic frequency range, 5 to 2400 Hz, and are ideal for detection of the low frequency noise generated by submarines and shipping traffic. Acoustic information is transmitted by a VHF Transmitter with transmission frequencies ranging from 136.0 to 173.5 MHz, divided into 99 programmable channels with 375kHz Spacing [77]. VHF output power is 1 W through a monopole whip antenna with a saltwater ground plane. The monopole antenna has an omnidirectional radiation pattern with an overhead null (Figure 3.14). This model is of a monopole whip antenna with an infinite

ground plane because the modeling software available was unable to model a saltwater ground plane. The saltwater ground plane creates a null near the surface of the water that will impact transmission at low elevation angles. The SSQ-53D sonobuoy's transmitter characteristics and antenna null has been studied and modeled by the Department of National Defence (DND) [78].

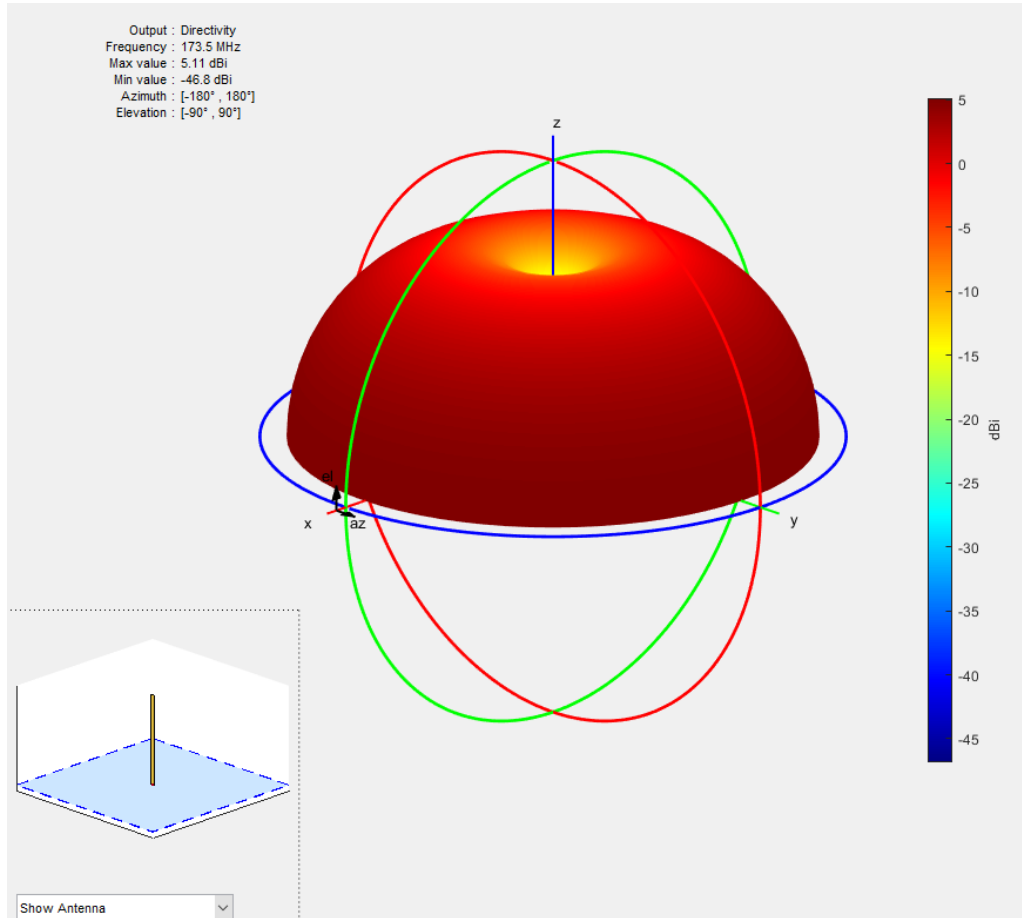


Figure 3.14 MATLAB model of a representative sonobuoy radiation pattern at 173.5 MHz [79]. Model uses a monopole whip antenna with an infinite ground plane. Output frequency of 173.5 MHz is upper bound of sonobuoy transmission range.

The SSQ-573 has similar specifications to the SSQ-53D but has an all-digital electronics design allowing for multiple communication modes. In addition to an analog low-noise DIFAR mode, it offers a high-dynamic range digital mode using a Gaussian Minimum Shift Keying (GMSK) modulation [80]. The GMSK modulation offers a data rate of 224 kbps. Geobuoys, also known as icepick-sonobuoys, are specifically designed for Arctic use and continue to be trialed by the CAF [81]. They have a large prong that penetrates the ice when air dropped (Figure 3.15). Rather than a conventional hydrophone, Geobuoys contain an omnidirectional geophone. The geophone detects underwater sounds, ambient noise, and ice movement from vibrations transmitted through the ice [82]. The radio

frequency (RF) transmission specifications are similar to the SSQ-53D sonobuoy. The Geobuoy allows for year-round data collection opportunities when ice coverage precludes the use of traditional sonobuoys.



Figure 3.15 Geobuoy in Arctic ice [81].

### 3.5 Sonobuoy placement

Placing sonobuoys in Lancaster Sound will present some unique challenges with ice coverage being a key consideration. Despite the presence of a polynya, the area is not completely ice free with drifting ice being pushed out into Baffin Bay. Even in areas of heavy ice coverage there exist small open water areas or ice leads through which a sonobuoy could be dropped. This requires a high degree of accuracy and will likely result in a significant rate of sensor damage [83]. For this reason, sonobuoys must be deployed in clear open water to prevent potential damage or entanglement. With only about three months of ice-free conditions, this seasonally limits air deployment of sonobuoys. Sonobuoys can also be deployed by ship, even in icy conditions, if dropped off the stern as the ship breaks through the ice. The frequent summer presence of Canadian Coast Guard (CCG) ice breakers presents additional opportunities for buoy deployment [70]. While there is still the possibility of damage to the electronics housing from drifting ice, deployment from icebreaking capable ships is a proven method [84]. When deployment of sonobuoys is impossible due to ice conditions, Geobuoys can be used. The portion of Lancaster Sound west of the formed ice arch consists of pack ice which is suitable for Geobuoy use until the ice arch collapses [40].

The sonobuoys will drift along with ocean currents. Maximum surface currents during the summer period are approximately 5 to 30 cm/s [37]. Assuming the current is uniform in the water column this gives an expected drift distance between satellite passes of 0.27 to 1.62 km for a satellite in low earth orbit. Total drift over the lifespan of the sonobuoy (8 hours) is 1.44 to 8.64 km. The full impact of sonobuoy drift cannot be determined until the precise orbit and pointing accuracy of the Audimus satellite is confirmed. Once the orbit is confirmed this can be modeled, however if buoy drift is a concern placement can be controlled. Deployment a location that maximizes coverage or to the northern side of Lancaster Sound where there is a weaker current can mitigate this.

## 4 Communications - Hydrophone to Audimus

This section provides an overview of general satellite communications theory and atmospheric effects on RF propagation. Signal propagation through the ionosphere is hindered by phenomenon unique to polar regions. The communication link between the sonobuoy and satellite is viable and largely governed by space path loss. The elevation angle is of critical importance for signal propagation and is defined by antenna characteristics.

### 4.1 Satellite Communications Theory

A specific communication link is necessary for any satellite mission. Satellite RF communication relies on the transmission of electromagnetic waves between satellites in space and ground-based receivers. In satellite communication electromagnetic (EM) waves propagate through space at the speed of light,  $c$  (m/s) from the transmitter on the ground to the satellite and vice versa. An EM wave can be represented by a sinusoidal plane wave, the general form of which is given by:

$$F(\vec{x}, t) = A \sin(2\pi f(\vec{x} \cdot \vec{n} - ct) + \phi) \quad (4.1)$$

where  $f$  is the frequency (Hz),  $A$  is the amplitude (m), and  $\phi$  phase shift (radians) [85], [86]. The amplitude, frequency, and phase may be adjusted to send information using the wave. This process of changing the wave properties is called modulation and is required to impart information on the carrier signal. There are a variety of modulation schemes used in satellite communications and the type used will be defined by the mission requirements.

Polarization refers to the orientation of the electric field vector of an EM wave. In satellite communication, linear polarization (horizontal and vertical) and circular polarization (right-hand and left-hand) are commonly used. The polarization of the transmitting and receiving antennas should be aligned for effective signal transmission and reception. A misalignment of polarization results in a reduction of received signal strength and is referred to as cross-polarization loss [87].

Antennas are essential components in satellite communication systems, responsible for transmitting and receiving RF signals. Many antenna types are available for satellite communications including simple wire antennas, Yagi antennas, parabolic antennas, and helical antennas. Antenna design will be determined by the specific requirements of the satellite communication system with key antenna design considerations including frequency of operation, gain, beamwidth, polarization, and radiation pattern. A well-designed communication system is critical to minimizing atmospheric effects and external noise while ensuring a stable communication link.

## 4.2 Atmospheric Effects

The primary source of atmospheric effects on the Audimus communication link comes from the ionosphere [88], [89]. The ionosphere is the ionized part of Earth's atmosphere affects RF signals propagating through it. Ionospheric attenuation, dispersion, and delay all disrupt signal propagation.

Due to the electron and ion content within, the ionosphere has a dielectric constant and conductivity that differs from free space. The ionosphere can therefore be described by its conductivity (mho/m),  $\sigma$  and relative permittivity,  $\epsilon'$ . These values are obtained from the ion density and collision frequency within the ionized region and are given by [88]:

$$\sigma = \frac{N_e q_e^2 \nu}{m_e (\omega^2 + \nu^2)} \quad (4.2)$$

and,

$$\epsilon' = 1 - \frac{N_e q_e^2}{\epsilon_0 m_e (\omega^2 + \nu^2)} \quad (4.3)$$

where  $N_e$  is the electron density (electrons/m<sup>3</sup>),  $q_e$  is the elementary charge ( $1.6 \times 10^{-19}$  C),  $\nu$  is the electron collision frequency (s<sup>-1</sup>),  $m_e$  is the electron mass ( $9 \times 10^{-31}$  kg),  $\omega$  is the angular frequency ( $2\pi f$  rad/s), and  $\epsilon_0$  is the permittivity of vacuum ( $8.854 \times 10^{-12}$  F/m). These formulations for conductivity and permittivity are used to estimate ionospheric losses for the communication link.

Faraday rotation is the rotation of the EM wave polarization as it propagates through a material subjected to a magnetic field. The interaction between the magnetic field of the wave and the material's electrons causes the propagating EM field components to experience different refractive indices. The difference in refractive indices for the polarized components causes them to travel at different speeds through the material and when recombined upon exiting the polarization is rotated by an angle relative to its original orientation [90]. The Faraday rotation angle  $\varphi$  (radians), is given by [89]:

$$\varphi = \frac{2.36 \times 10^4}{f^2} B TEC \quad (4.4)$$

where  $f$  is the frequency (Hz),  $B$  is the average Earth magnetic field (Wb/m<sup>2</sup>), and  $TEC$  is total electron content (electrons/m<sup>2</sup>). Total electron content is required for estimation of several ionospheric effects and is derived from the electron concentration along the propagation path between the transmitter and receiver. Electron concentration depends on a variety of factors including altitude, geomagnetic latitude, diurnal cycle, and solar activity. TEC is the number of electrons within a column one square meter in cross section, with a vertical or zenith path most often used[91]. For estimation of satellite communication path effects a recommended maximum value of  $1 \times 10^{18}$  electrons/m<sup>2</sup> may

be used [89]. This assumes a zenith path with a cross-section of  $1 \text{ m}^2$ . TEC varies widely in polar regions and the maximum value is used to account for the worst possibility.

In addition to the ionosphere, the neutral, non-ionized atmosphere also affects the propagation of EM waves. Atmospheric conditions, such as moisture content, temperature, and pressure, can cause absorption and scattering of RF signals. The primary contributors to absorption are oxygen and water. Neutral atmosphere absorption is generally low for signals in the VHF range and is given by.

$$L_{atm} = \frac{16\gamma_o}{\sqrt{\sin^2(\epsilon) + 16/a + \sin \epsilon}} + \frac{4\gamma_w}{\sqrt{\sin^2(\epsilon) + 4/a + \sin \epsilon}} \quad (4.5)$$

where  $\epsilon$  is the elevation angle (radians),  $\gamma_o$  is the specific attenuation coefficient for oxygen (dB/km),  $\gamma_w$  is the specific attenuation for water vapour (dB/km), and  $a$  is the effective earth radius [88]. The factor  $a$  is given by  $a = kR_e$ , where the radius of the Earth  $R_e$  is modified by a straightening factor  $k$  that accounts for the curvature of the earth [88]. For frequencies in the VHF band  $\gamma_o$  and  $\gamma_w$  are small, ( $< 0.1 \text{ dB}$ ). Rain, fog, and ice crystals can cause attenuation at higher frequencies but are negligible in the VHF band.

One of the most severe disruptions along ionospheric propagation paths for signals below 3 GHz is caused by ionospheric scintillation [91]. Ionospheric scintillation refers to the rapid fluctuations in the amplitude and phase of radio signals as they pass through irregularities in the ionosphere. Scintillation is most severe in norther latitudes with peak activity in the auroral and polar regions [89]. Scintillation events are more frequently observed during nighttime and occur more frequently and more intense around the local magnetic zenith [92]. Scintillation events are generally short lived lasting from 30 minutes to a few hours. Scintillation is characterized by the scintillation index,  $S_4$  and is related to peak-to-peak intensity fluctuations of the received signal. In Artic regions phase scintillation, is more pronounced than amplitude scintillation with approximately 90% of scintillation events having a  $S_4 < 0.25$  [92]. This equates to a peak-to-peak fluctuation or depth of scintillation fading of 4.8 dB [91].

Auroral and polar cap absorption are ionospheric phenomena unique to high latitude regions and should be considered for Audimus. Auroral absorption is the increased attenuation of radio signals passing through the Earth's ionosphere in regions where auroral activity is present, centered close to the latitude of maxim occurrence of visual aurorae [91]. Primarily affecting the VHF band, it occurs when incident energetic electrons cause increased electron density in the ionosphere. This can disrupt satellite communications with increased signal attenuation. They occur irregularly but are generally short in duration with an average of 30 minutes [93]. Losses for auroral absorption in the VHF range are typically on the order of 3 dB or less.

Polar cap absorption occurs at latitudes above  $60^\circ$  during times of increased solar activity. It usually occurs as discrete events associated peak periods of sunspot activity and results in significant absorption of radio waves at frequencies below 200 MHz [93]. The duration of polar cap absorption is greater than that of auroral absorption but still relatively short

lived, on the order of days. A comprehensive model is not available however estimated effects show up to a 5 dB loss in signal during such events [94]. These ionospheric phenomena require consideration when determining the satellite link budget.

### 4.3 Link Budget

A satellite link budget is a comprehensive analysis of the communication link between the satellite and associated ground stations. It examines all the gains and losses of the communication signal to determine the feasibility of the communication link. The process for calculating link budgets is well established [90], [95]. Since the final specifications of the primary hydrophone system are not known, a link budget analysis of the SSQ-573 DIFAR sonobuoy digital mode transmission to Audimus follows. Sonobuoys represent the minimum power option for transmitting acoustic data and a viable link with these specifications will ensure effective communications with the higher powered systems later. The sonobuoy specifications outlined in Section 3.4 are used. Both the minimum frequency of 136.0 MHz and maximum frequency of 173.5 MHz are considered.

The link budget determined by the signal to noise ratio (SNR) in a receiver and is based on the received carrier power ( $P_r$ ) and the receiver noise power ( $N$ ) which are given by:

$$P_r = EIRP + G_r - L_s - L_a - L_{ta} - L_{ra} \quad (4.6)$$

where  $EIRP$  is the effective isotropic radiated power,  $G_r$  is the gain of the receiving antenna,  $L_s$  is space path losses,  $L_a$  is atmospheric losses,  $L_{ta}$  is losses from the transmitting antenna, and  $L_{ra}$  is losses from the receiving antenna [90].

$$N = k + T_s - B_n \quad (4.7)$$

where  $k$  is Boltzmann's constant,  $T_s$  is the system noise temperature, and  $B_n$  is the noise bandwidth of the receiver [90]. The  $EIRP$  is given by:

$$EIRP = P_t + G_t - L_l \quad (4.8)$$

where  $P_t$ ,  $G_t$  and  $L_l$  is the transmission power, gain of the transmitting antenna, and system line losses respectively. Using a  $P_t$  of 1 W (0 dB),  $G_t$  of 5.07 dB and  $L_l$  of 0.5 dB gives an EIRP of 4.57 dB [78]. The receiving antenna gain will be determined later with the final spacecraft design. Small satellites operating in the VHF range typically use dipole whip antennas due to their simplicity and effective omnidirectional radiation pattern. For these calculations the nominal value for a dipole,  $G_r= 2.15$  dBi, is used [96]. Antenna gain is often compared to an ideal isotropic antenna with units of dBi used to represent the relative measure of directional gain. This allows the standardization of measurements in communication systems and simplifies calculation of the link budget.

Next we calculate the various transmission losses beginning with the space loss  $L_s$ . The distance  $d$  between the sonobuoy and satellite for a given elevation angle  $\epsilon$  is given by:

$$d = -R_E \sin(\epsilon) + \sqrt{R_E^2 \sin^2(\epsilon) + 2hR_e + h^2} \quad (4.9)$$

with  $R_E$  the radius of the earth and  $h$  the satellite altitude. Since the Earth is an oblate spheroid and Audimus will be in a polar orbit the polar radius is used where  $R_E$  is 6356 km [97]. To account for the worst-case scenario the upper end of the planned satellite altitude is used. For an altitude of 600 km,  $d$  is 2826.2 km when  $\epsilon$  is  $0^\circ$  for horizon-to-horizon communications. However, due to the antenna null at low elevation angles caused by the saltwater ground plane of the sonobuoy, horizon-to-horizon comms are unlikely and a higher elevation angle is required [78]. An  $\epsilon$  of  $10^\circ$  is used because measurements of the DIFAR sonobuoy beam patterns indicate a significant null below this angle. The loss of gain below this angle reduces the link budget enough to prevent effective communication. This gives a  $d$  of 1930.3 km. Space path loss is then given by:

$$L_s = \left( \frac{4\pi d}{\lambda} \right)^2 \quad (4.10)$$

where  $\lambda$  is the signal wavelength (m) and  $d$  is given by Equation (4.9) [90]. The highest sonobuoy frequency  $f_{max}$  of 173.5 Hz gives the maximum space loss 142.9 dB. For the minimum  $f_{min} = 136.0$  Hz  $L_s = 140.8$  dB.

Atmospheric losses  $L_a$  are a combination of ionospheric,  $L_{ion}$  and neutral atmospheric losses,  $L_{atm}$ . Ionospheric losses are given by [88]:

$$L_{ion} = 10 \log(1 - \alpha d) \quad (4.11)$$

with  $\alpha$  the attenuation factor defined by:

$$\alpha = \frac{60\pi\sigma}{\sqrt{\epsilon'}} \quad (4.12)$$

where  $\sigma$  and  $\epsilon'$  are given by Equations (4.2) and (4.3) respectively. The value for electron density in Arctic regions may be obtained using CHAIM, however this model is known to underestimate electron densities, so the peak value measured at resolute bay is used,  $N_e = 3 \times 10^{11}$  [50]. Equation (4.11) gives  $L_{ion} = 0.05$  dB for  $f = 173.5$  MHz and  $L_{ion} = 0.09$  dB for  $f = 136.0$  MHz.

Equation (4.5), the neutral atmosphere absorption can be reduced for  $\epsilon \geq 10^\circ$  to:

$$L_{atm} = \frac{8\gamma_o + 2\gamma_w}{\sin(\epsilon)} \quad (4.13)$$

The values for  $\gamma_o$  and  $\gamma_w$  for water vapour can be extrapolated giving a  $\gamma_o$  of  $6.5 \times 10^{-3}$  dB km $^{-1}$  and a  $\gamma_w$  of 0 dB km $^{-1}$  for the VHF band [88]. Again using  $\epsilon$  of  $10^\circ$  gives  $L_{atm} = 0.3$  dB. Attenuation due to rain and fog are negligible in the VHF band and are assumed to be zero in this analysis [88]. Combining  $L_{ion}$  and  $L_{atm}$  gives an  $L_a$  of 0.35 to 0.39 dB.

Transmitting antenna losses,  $L_{ta}$ , consist of pointing losses and polarization mismatch losses. Since the sonobuoy uses a quarter-wave monopole antenna there is a null along the axis of the monopole (Figure 3.14), however since the satellite will rarely fly directly overhead and sonobuoy deployment can be controlled to ensure maximum gain, off-axis is assumed to be zero. Polarization mismatch loss occurs when the polarization state of the receiver is not perfectly matched to the polarization of the incoming wave. The effects of Faraday rotation in the ionosphere at VHF frequencies make linear links impractical. Using Equation (4.4), the Faraday rotation for the sonobuoy is 45.5 rad. To combat this offset a circularly polarized antenna may be used. When a linear-circular link is used, the polarization mismatch loss is 3 dB [98]. Since the sonobuoy antenna is linearly polarized Audimus will use a circular polarization giving  $L_{ta} = 3.0$  dB.

Receiving antenna losses  $L_{ra}$  consist of pointing losses, which are again assumed to be zero, and transmission line losses. Line losses will not be known until the final satellite configuration is confirmed so an assumed value of 1 dB is used giving  $L_{ra} = 1.0$  dB. Combining these values into Equation (4.6) gives the received carrier power,

$$P_r = -140.5 \text{ dB} \quad (4.14)$$

Similar calculations performed for the SSQ-53D Sonobuoy and the Geobuoy are summarized below in Table 4.1. Calculations for a transmission frequency of 136.0 MHz are summarized in Table 4.2. Notable differences occur in EIRP are due differing power output and antenna gain values. The Geobuoy offers a noticeable reduction in polarization mismatch due to its circularly polarized antenna assuming circular-circular configuration. There is a consistent 2 dB difference between the highest and lowest transmission frequency.

Sonobuoy	EIRP (dB)	$G_r$ (dB)	$L_s$ (dB)	$L_a$ (dB)	$L_{ta}$ (dB)	$L_{ra}$ (dB)	$P_r$ (dB)
SSQ-537	4.57	2.15	142.9	0.35	3.0	1.0	-140.6
SSQ-53D	2.45	2.15	142.9	0.35	3.0	1.0	-142.7
Geobuoy	3.26	2.15	142.9	0.35	0.2	1.0	-139.0

Table 4.1 Satellite received carrier power for sonobuoy transmission of 173.5 MHz

Sonobuoy	EIRP (dB)	$G_r$ (dB)	$L_s$ (dB)	$L_a$ (dB)	$L_{ta}$ (dB)	$L_{ra}$ (dB)	$P_r$ (dB)
SSQ-537	4.57	2.15	140.8	0.39	3.0	1.0	-138.6
SSQ-53D	2.45	2.15	140.8	0.39	3.0	1.0	-140.6
Geobuoy	3.26	2.15	140.8	0.39	0.2	1.0	-137.0

Table 4.2 Satellite received carrier power for sonobuoy transmission of 136.0 MHz

System noise temperature,  $T_s$  is based upon the antenna noise temperature. For an omnidirectional spacecraft antenna, this can be approximated as half the Earth's radio temperature, 145 K [99]. Converting to decibels gives  $T_s = 21.6$  dB.

The noise bandwidth,  $B_n$  is determined by the required receiver bandwidth. Sonobuoy transmissions use a wide bandwidth of approximately 230 kHz [78]. Converted to decibels this is  $B_n = 53.5$  dB. Boltzmann's constant,  $k$  in dB is -228.6. Using these values in Equation (5.7) gives a final system noise power of  $N = -153.5$  dB. This value is

independent of the transmitter and is the same for all sonobuoys. The signal-to-noise ratio at the receiver,  $SNR$  is given by:

$$SNR = P_r - N = -140.5 - (-153.5) = 13.0 \text{ dB} \quad (4.15)$$

While the calculation of SNR, where noise power is considered over the entire bandwidth, is appropriate for analog signals, most modern satellite applications use digital signals. In digital signals the noise is considered per bit and is represented by the ratio of received energy per bit to noise density ratio,  $E_b/N_o$ . The  $E_b/N_o$  required is determined by the bit error rate (BER) [87]. For most near-earth missions, a BER of  $10^{-5}$  is standard and this will be used by Audimus. The calculated  $E_b/N_o$  is then given by:

$$E_b/N_o = EIRP + G_r + k - L_s - L_a - L_{ta} - L_{ra} - R \quad (4.16)$$

where R is the link data rate (dB) and all other parameters are as defined above. For the SSQ-537 sonobuoy the data rate is 224 kbps or 53.5 dB. This gives an  $E_b/N_o$  of 12.9 dB. For the SSQ-537 the required  $E_b/N_o$  for GMSK modulation is 9.8 dB giving a link margin of 3.1 dB, just above the standard margin of 3 dB for satellite communications. Since the SSQ-53D and Geobuoy use analog Frequency Modulation (FM), there is no defined threshold for a margin, however wideband FM can operate with SNR's as low as 5 to 10 dB [90]. The calculated SNR for the analog buoys is greater than 10 dB suggesting that the link is viable. Final SNR and link margin numbers for the sonobuoy to Audimus link are summarized below (Table 4.3). These number represent the worst-case values for  $f=173.5$  MHz while for  $f=136.0$  MHz the link margin is 2 Db greater. This shows the impact of space path loss for the higher frequency is greater than the atmospheric effects at the lower frequency. The preferred frequency for sonobuoy use is therefore 136.0 MHz or the lowest authorized frequency available.

Sonobuoy	$P_r$ (dB)	N (dB)	$E_b/N_o$ (dB)	Required $E_b/N_o$ (dB)	SNR (dB)	Required SNR (dB)	Margin (dB)
SSQ-537	-140.5	-153.4	12.9	9.8	n/a	n/a	<b>3.1</b>
SSQ-53D	-142.7	-153.5	n/a	n/a	10.8	10 dB	<b>0.8</b>
Geobuoy	-139.0	-153.5	n/a	n/a	14.5	10 dB	<b>4.5</b>

Table 4.3 Summary of calculated and required  $E_b/N_o$  and SNR with link margin for all sonobuoys.  $f=173.5$  MHz.

#### 4.4 Additional Link Considerations

Ionospheric refraction also impacts signal propagation through the ionosphere by inducing a time delay and corresponding satellite orbital position offset [100]. The different layers of the ionosphere have different refractive indices. As the RF waves pass through these layers the wave is bent. The critical angle is the maximum angle of incidence that results in a refracted wave, beyond this the signal is reflected back to the surface [88]. The critical angle is a function of the signal frequency  $f$ (Hz) and electron density in the ionosphere  $N_e$  (electrons/m<sup>3</sup>). The critical angle  $\phi_c$  is given by:

$$\phi_c = \sin^{-1} \left( \sqrt{1 - \frac{80.5N_e}{f^2}} \right) \quad (4.17)$$

The critical frequency is calculated when the critical angle is zero. The critical frequency  $f_{co}$  (Hz) needed to pass through the ionosphere, assuming a vertical zenith angle of incidence, is given by:

$$f_{co} = \sqrt{80.5N_e} \quad (4.18)$$

The critical frequency is influenced by the number of sunspots by:

$$f_c = f_{co}(1 + aR) \quad (4.19)$$

where  $a$  is a constant determined by the ionospheric region and  $R$  is the number of sunspots [88]. The incident angle  $\phi$  also influences the critical frequency by:

$$f_c = f_{co} \sec \phi \quad (4.20)$$

Combining these gives the maximum satellite zenith angle at which communication can still occur:

$$\phi_{max} = \cos^{-1} \left( \frac{f_{co}(1 + aR)}{f_c} \right) \quad (4.21)$$

Using  $N_e = 3 \times 10^{11}$  for the Arctic,  $R = 122.5$  for 2026, and  $a = 0.01$  for the F<sub>1</sub> layer give a maximum satellite zenith of  $\phi_{max} = 86.4^\circ$  for the sonobuoy signal at the upper frequency of  $f = 173.5$  MHz. For the lower sonobuoy frequency of  $f = 136.0$  MHz this decreases to  $\phi_{max} = 85.4^\circ$  or a minimum elevation angle  $\epsilon_{min} = 4.6^\circ$ . This is well below the elevation angle required due to the sonobuoy monopole antenna null; thus the antenna null and not ionospheric refraction will be the limiting elevation angle.

The orbital velocity of the satellite will cause a Doppler shift in the received sonobuoy signal. Orbital velocity of a satellite is a function of altitude and given by [101]:

$$v = \left( \mu \left( \frac{2}{R_{sat}} - \frac{1}{a_{sat}} \right) \right)^{1/2} \quad (4.22)$$

where  $\mu$  is the gravitational parameter  $\mu = 3.98 \times 10^5 \text{ km}^3/\text{s}^2$ ,  $R_{sat}$  is the radial distance to the satellite from the center of the Earth (km), and  $a_{sat}$  is the satellite's semi-major axis (km). Using  $R_{sat} = R_E + a = 6956$  km and  $a_{sat} = R_{sat}$  for a circular orbit gives  $v = 7.6$  km/s. For a satellite passing directly over an observer the Doppler shift is given by:

$$f_D = \frac{vf}{c} \sin \theta \quad (4.23)$$

where  $v$  is given by Equation (4.22),  $f$  is the frequency of the sonobuoy (Hz) [88]. The Doppler shift for the full range of sonobuoy frequencies is shown in Figure 4.1.

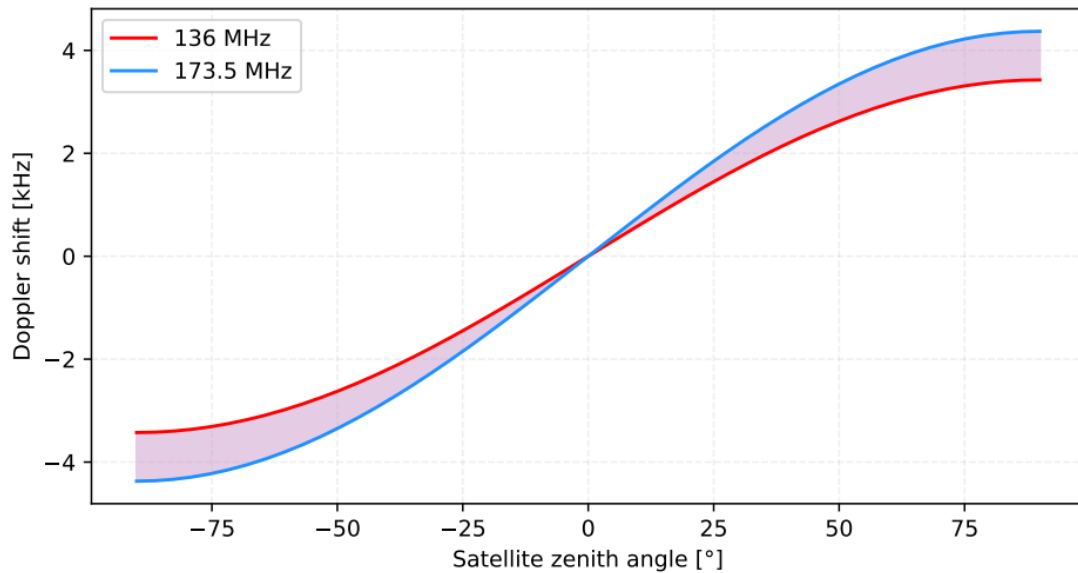


Figure 4.1 Doppler shift of sonobuoy frequency band 136.0 MHz to 173.5 MHz [100]. Horizon-to-horizon overhead pass for 600 km orbit.

Equation 4.23 assumes an overhead pass, however there will be less Doppler shift if the satellite is offset from the sonobuoy, which will often be the case due to the overhead antenna null. In addition to the frequency shift the rate of change is also considered. LEO satellites travel at approximately 7.8 km/s causing the frequency shift to vary within seconds. The rapid rate of change presents challenges for the RF receiver to adapt quickly enough [90]. While generally small in the frequency range sonobuoys use, it must still be accounted for when analyzing the acoustic data. Since the sonobuoy data is contained in the RF signal correcting for the doppler shift must be done before demodulation as even small shifts may provide erroneous data [102]. Doppler effects can be corrected with automatic frequency control, compensation algorithms and appropriate modulation and demodulation schemes [103].

Beyond the link budget an additional margin to account for the ionospheric effects outlined section 4.2 is required. At mid latitudes this is typically an additional 2 dB but should be higher for polar regions [90]. The maximum loss for ionospheric effects was shown to be 5 dB making this the additional margin required. There is insufficient room in the link margin to allow for this, so during periods of high solar activity and increased ionospheric effects, reception of the sonobuoy signal with Audimus may not be possible. With the link budget confirmed, the payload appropriate for signal reception can now be defined.

## 5 High Altitude Balloon Mission

This section discusses an experimental high altitude balloon mission designed to simulate the Audimus mission. System design was constrained by radio regulations and commercially available equipment. Successful data collection occurred throughout the mission with minimal atmospheric losses.

### 5.1 Description of Mission

In July 2023, I along with other students from the Natural Sciences and Engineering Research Council of Canada (NSERC) Collaborative Research and Training Experience program (CREATE) International Space Mission (ISM) Training Program launched two high-altitude research balloons [104]. One balloon collected a variety of atmospheric measurements while the other carried a VHF relay. This project was intended as a proof of concept for the future RMC CubeSat, Audimus.

The primary objective for the VHF Relay Balloon was to perform a basic simulation of ground-based Sonobuoy RF transmission to a space-based receiver. A single ground station acted as both a simulated sonobuoy and as a simulated RMC ground station. The simulated sonobuoy ground station emitted a VHF transmission at fixed time intervals determined by the Global Positioning System (GPS) clock. The transmission contained a call sign, packet identifier, and an audio clip. The radio on the balloon received and stored the transmission along with a GPS location and timestamp. The balloon radio then re-transmitted the packet in UHF to the ground station that received and stored the relayed transmission. While the students were not able to faithfully replicate a sonobuoy RF transmission, the balloon mission did provide valuable insight into how the Audimus mission could develop.

### 5.2 System Design

Two handheld BaoFeng UV-5R radio handsets were repurposed to act as the ground station and balloon radios [105]. This was due to regulations surrounding the construction of radios that utilize amateur radio (HAM) bands, as none of the team members held the required licence. A custom L-shape dipole antenna was constructed and tuned for use on the balloon payload. A commercial off-the-shelf (COTS) dual band antenna was used as the ground station radio. The onboard computer (OBC) selected for the VHF Relay was a Raspberry Pi 4. The Raspberry Pi facilitated the audio recording and storage while a GPS chip provided clock discipline for accurate timing. The conceptual layout is shown in Figure 5.1. Once assembled payload components were placed inside a foam container for protection (Figure 5.2).

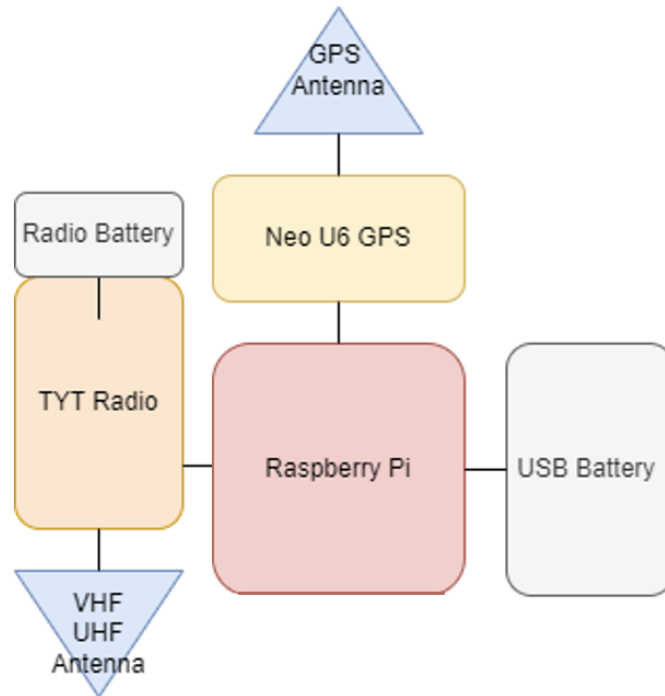


Figure 5.1 Balloon relay system layout components and conceptual layout.

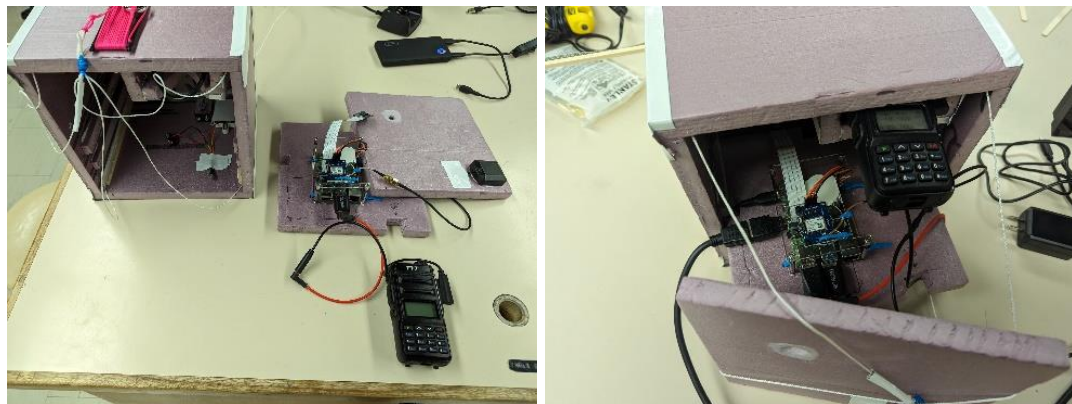


Figure 5.2 VHF relay balloon payload prior to final assembly.

The L shape dipole antenna was constructed with pole lengths of approximately 0.5 m. This antenna served as a one quarter wave receiver for the uplink VHF signal from the ground station and as a three-quarter wave transmitter for the UHF downlink signal. The antenna was constructed out of a length of RG-58/U co-axial cable with an impedance of 50 ohms. The outer PVC jacket of the cable was stripped 0.5 m from one end of the cable and the internal bare copper conductor was separated from the tinned copper braid shield of the outer conductor (Figure 5.3).

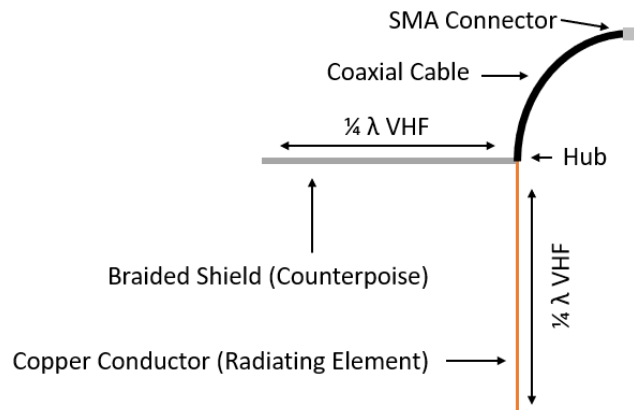


Figure 5.3: Dual band VHF/UHF L shape dipole antenna.

The two poles were fixed to the payload forming a 90-degree angle with one another, with the copper radiating element extending to the nadir, and the counterpoise attached to a horizontal wooden beam extending from the payload. Computer simulations using 4NEC2 software predicted that an L shape dipole antenna in this configuration would produce a tilted cardioid radiation pattern, adequate for transmission to and from a vertically polarized ground-based antenna at the elevation angles expected. Figure 5.4 shows a computer simulation of the expected radiation pattern of a general L shape dipole antenna. Time did not permit detailed frequency specific modeling of the payload antenna.

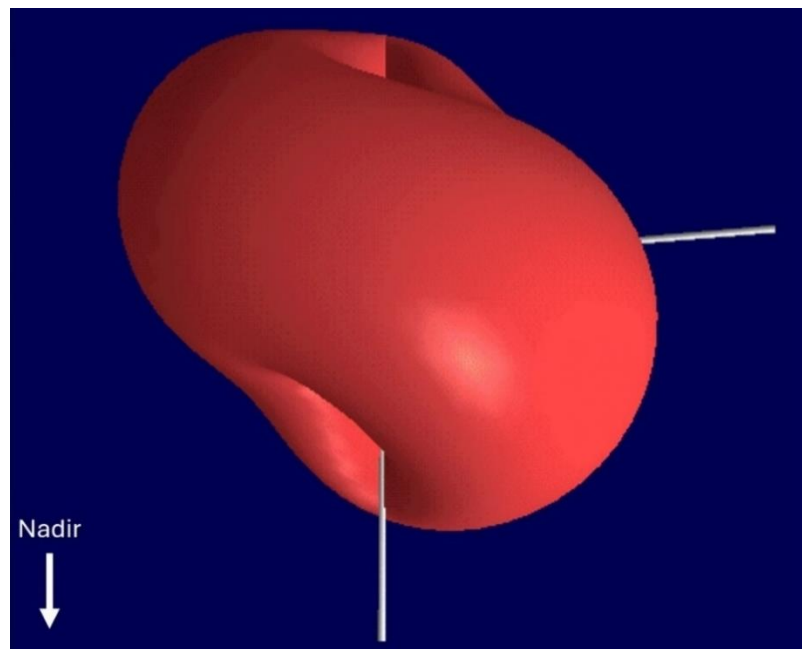


Figure 5.4: 4NEC2 Software simulation of a radiation pattern for an L shape dipole Antenna [106].

The ground station utilized a COTS Nagoya UT-308UV 22-inch whip antenna. It was fixed to the top of a vehicle that provided a ground plane virtual surface to improve antenna performance. The COTS antenna was attached via an SMA connector to a modified handheld HAM radio. This handheld radio interfaced directly into a Raspberry Pi, like the payload radio. The ground station radio was programmed to transmit on a 146.580 MHz frequency and receive on a 439.740 MHz UHF frequency. The VHF transmit power of the radio was set to low, which was measured to be 1.1 W. A NEO-6M GPS module was also interfaced with the Raspberry Pi to provide clock discipline for timing the radio transmission (Figure 5.5).

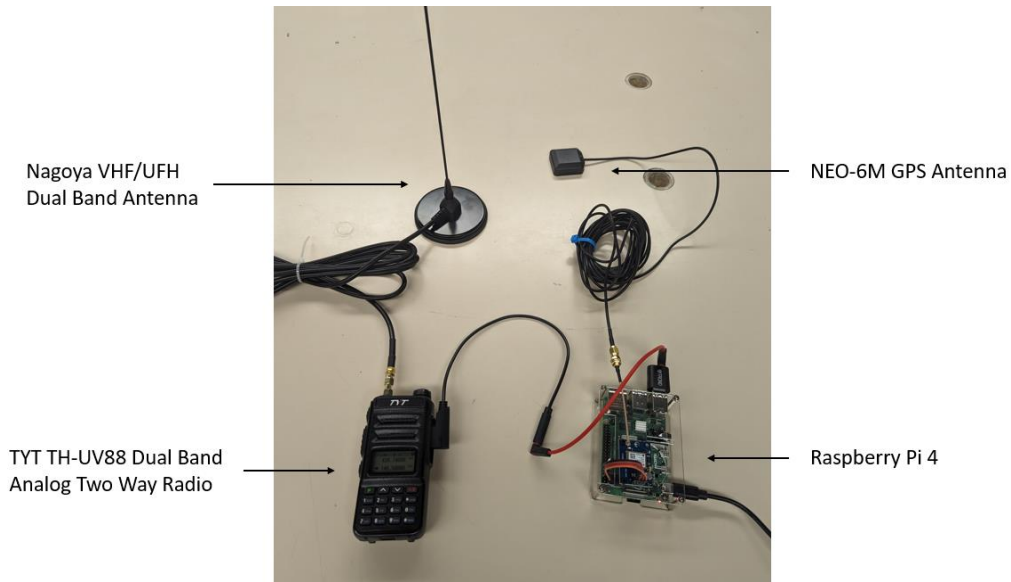


Figure 5.5: Ground station for the VHF relay balloon mission.

### 5.3 Data Collection

The data communicated was a pre-recorded 16 bit .WAV audio file transmitted at 8000 Hz, with the objective of exploring how the audio quality changed as the radios separated. Since both radios were required to send and receive, a timing-based solution was implemented. For scheduling the Raspberry Pi-clocks were disciplined using GPS to ensure that the ground station and balloon computers were synchronized in their radio transmission and reception. The GPS provided proper timing but an error prevented the logging of positional data. A backup Automatic Packet Reporting System (APRS) was attached externally to the payload and was used for tracking and mission reconstruction. The audio file was transmitted from the ground station over the VHF band, it was received and recorded by the balloon payload. The recorded message was subsequently transmitted back to the ground station over UHF and again recorded by the OBC for later analysis. A complete transmission cycle was conducted every minute for the duration of flight.

The VHF relay system worked well throughout the flight. Nearly all VHF and UHF transmissions were received with few missed transmissions. The majority of missed

transmissions occurred just prior to the payload impacting the ground on decent when the ground station lost line of sight with the relay. A qualitative analysis of the recorded audio showed the quality of the recordings to be consistent over the mission duration with no obvious losses. During flight the balloon reached a maximum altitude of 31 km with a maximum slant range of 84 km. Figure 5.6 shows the complete flight path of the balloon as recorded by the APRS tracking module. Link budget calculations showed there should be little difficulty communicating over this distance and this was demonstrated by the mission. A quantitative analysis of the audio files using software to determine precise signal losses follows.



Figure 5.6 Flight path of the VHF relay balloon

## 5.4 Data Analysis

Audacity, an open-source program for editing audio was used to analyze the recorded files [107]. A baseline recording was taken prior to launch with the balloon payload adjacent to the ground station. Subsequent recordings are compared against the baseline and visualized using the software (Figure 5.7). Examination of the spectrograms showed the quality of audio recordings to be consistent over the duration of the mission with little obvious losses. Using Audacity, the recordings were broken down with the frequency analysis tool to create a spectrum plot (Figure 5.8).

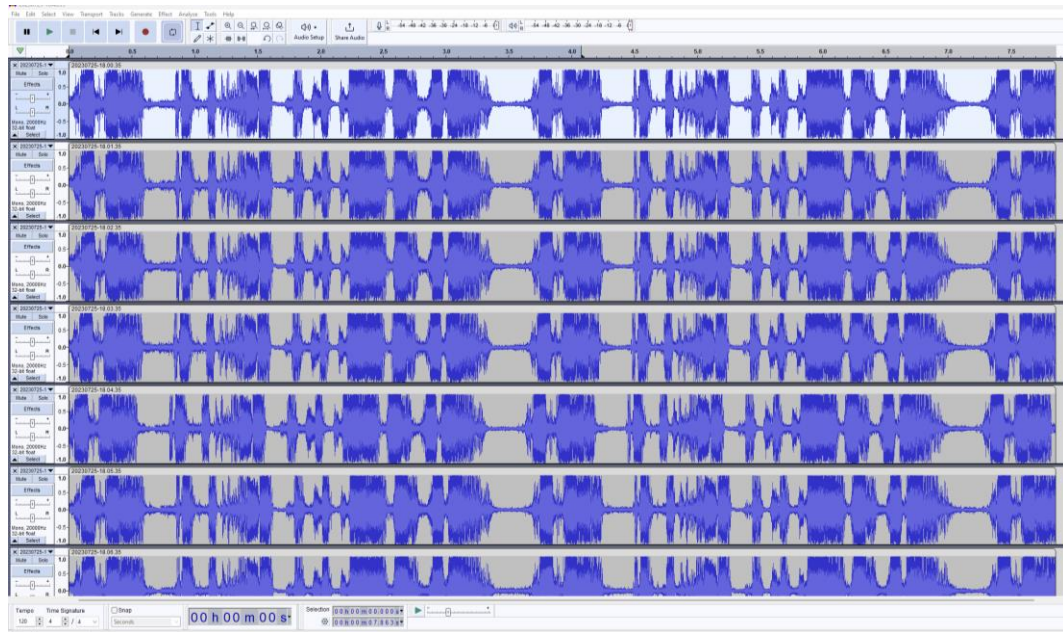


Figure 5.7 Audacity interface showing spectrum comparison of multiple recordings with baseline recording (top row). The vertical axis shows amplitude while the horizontal axis shows time.

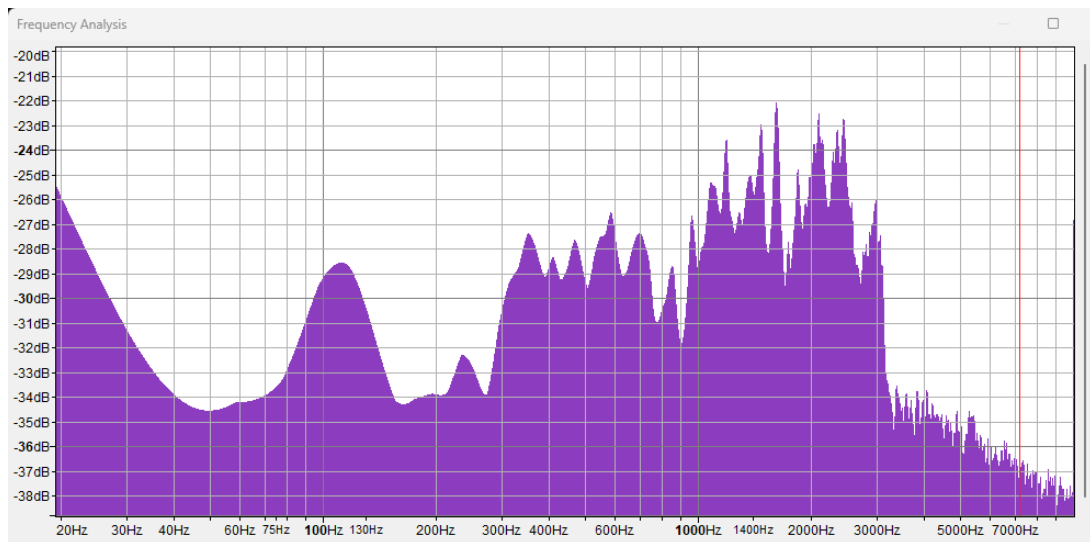


Figure 5.8 Resultant spectrum plot of a single recording using the frequency analysis in Audacity.

For each frequency in the plot, the dB level is compared to baseline spectrum to determine the change in decibel (dB) level and then averaged for each recording. This is done for each recording over the entire flight time. Since the recordings are compared against other recordings rather than the recorded audio files equipment losses are not considered. The resulting data is presented in Figure 5.9. The dB losses gradually increase as the distance

from the ground station increases. Average losses range from .001 dB post launch to .35 dB at peak range with outliers as high as 4 dB. The cause of these outliers is believed to be the spinning of the antenna null as the balloon climbed but insufficient data was collected for the necessary analysis. The losses observed during the relay mission are smaller than expected and do not fully account for free space path loss. Extrapolating the trendline to a slant range of 2000 km shows only a loss of 28 dB compared to the expected 142 dB.

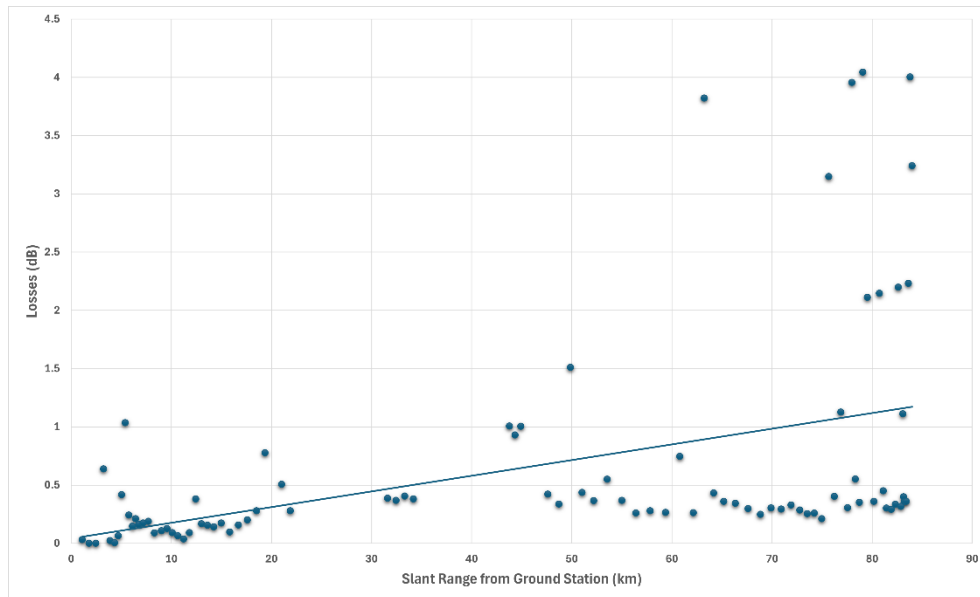


Figure 5.9: Losses in VHF recording shown with increasing slant range. Linear trendline shows increasing slope.

Signal reception was consistent over the course of the mission with minimal losses observed but the data analysis is inconsistent with expected losses. A timing-based solution for reception and transmission de-confliction was effective and could be adapted for Audimus. While not an exact parallel, the success of the balloon relay suggests the concept is feasible at greater altitudes and the concept for Audimus is sound.

## 6 Audimus Payload

This section outlines the Audimus payload requirements and characteristics. Specific transmission and bandwidth requirements from sonobuoy transmitters dictate system design. Advances in software defined radios (SDR) provide a novel solution.

### 6.1 Requirements

The unique mission and operating environment necessitate specific payload requirements. The primary payload for Audimus is a VHF receiver and antenna optimized for reception of sonobuoy signals, 136.0 MHz to 173.5 MHz [108]. The main hydrophone systems will have the same requirements as a sonobuoy to ensure all potential data sources can be detected by a single receiver. Older sonobuoys like the SSQ-53D and Geobuoy require an analog FM receiver, while newer models such as the SSQ-573 are capable of digital modulation [77], [80].

Both analog and digital buoys necessitate a wide signal bandwidth, 230 kHz, while the 99 channels over the given frequency range require a multi-channel receiver. The 230 kHz bandwidth is the occupied bandwidth, the bandwidth within which 99% of the output power is contained [78]. In actuality the bandwidth occupied by the acoustic data is much narrower than this with a carrier frequency deviation of  $\pm 40$  kHz [102]. The receiver also needs a sufficiently high sample rate, 48 kHz for analog DIFAR buoys and 96 kHz for newer GPS enabled buoys [109], [110]. While these sample rates are too low for the full occupied bandwidth band pass filters can be used to recover the acoustic data and prevent anti-aliasing [111], [112].

The data rate for the SSQ-573 in digital mode is 224 kbps with GMSK modulation [80]. In addition to the analog requirements the receiver should also be able to receive the digital signal and sample it at an appropriate rate. Data storage also needs to be considered. Software simulation estimates 14 passes over Lancaster Sound but only 6 over RMC necessitating a store and forward architecture [113]. Given the 224 kbps data rate for the SSQ-573 and an average pass length of 583s gives 230 MB of data collected daily.

The antenna needs to be omnidirectional and circularly polarized to compensate for the effects of Faraday rotation on the incoming signal and ensure reception. Receiver antenna gain is important to receive the weak sonobuoy signals of only 1 W of output power. To minimize project risk COTS products with flight heritage will be used. All products chosen must also adhere to the CubeSat design specification [114].

### 6.2 Receiver Systems

A survey of available COTS receivers revealed few options meeting the specified requirements [115], [116], [117]. While VHF is widely used, and one of the most mature bands in CubeSat communications, digital modulation schemes are almost exclusively

used [118]. The VHF receivers that were available offered only limited bandwidth and data rates unsuitable for the Audimus mission [119]. The only receivers to offer a larger bandwidth were SDR's. SDR's have the radio's functions implemented in Digital Signal Processing (DSP) software rather than hardware. They offer greater flexibility allowing them to be used with multiple bands, filtering, adaptive modulation, and coding schemes [118]. SDRs are especially attractive for use on CubeSats. They are becoming increasingly small and efficient as electronics become smaller, with multiple flight tested systems available [118], [120]. An SDR will offer the required frequency, bandwidth, data rate, and modulation for the Audimus mission while having the additional flexibility of reconfiguration in flight. The TOTEM SDR from Alén Space is one such system available for Audimus (Figure 6.1). The TOTEM exceeds the specifications required for Audimus, operating between 70 MHz and 6 GHz with up to a 56 MHz bandwidth and multiple transmit and receive interfaces. It has flight heritage and meets all design specifications since it is purpose built for use on CubeSats.



Figure 6.1 TOTEM SDR with wideband transceiver [121].

CubeSat VHF antenna options are similarly limited. A survey of available systems provided only one suitable option for Audimus, the CubeSat antenna system from ISISSPACE [122]. The deployable CubeSat antenna system from ISISSPACE is the only VHF COTS antenna available. It offers the necessary bandwidth and with four individual antennas can be used in a turnstile configuration for a circular polarization (Figure 6.2).

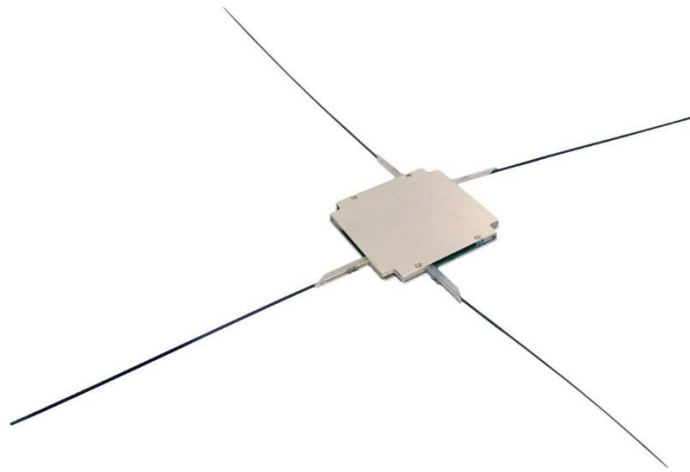


Figure 6.2 ISISSPACE deployable CubeSat Antenna System for 1U/3U CubeSats [122].

## 7 Audimus Operations

This section outlines details of the Audimus mission including testing the primary payload, mission operations, and mission continuation. A robust test plan supported by DRDC will ensure success at all stages. Downlink limitations may lead to a loss of data but will not hinder mission success. The Audimus mission will inform future research and follow on missions.

### 7.1 Communications Testing

The Audimus mission is scheduled for launch in early 2026, with assembly, integration and testing (AIT) occurring in 2025. An extensive test plan for the payload and primary mission objective, supported by DRDC, will be implemented both before and after launch. Prior to assembly, computer simulations to confirm the validity of the link calculations will be conducted. The open-source software GNURadio will be used to degrade the SNR of sonobuoy recordings and assess the results [123]. Sonobuoy recordings have been provided by DRDC. Once satellite assembly begins, DRDC will provide the Audimus team with an Ultra bouy-in-a-box system (BIBS). This system consists of the upper portion of the sonobuoy components, including the signal processing and RF transmitter, in a portable case to support laboratory bench testing. The BIBS will be used to test RF reception of the payload during AIT.

Once Audimus is launched, DRDC will continue to support a staged sonobuoy testing plan. Following satellite commissioning in orbit DRDC will use a sonobuoy simulator for communication trials from the DRDC Atlantic location in Halifax. Once the payload is confirmed to be operational, sonobuoys will be deployed off the coast of Halifax. Upon successful communication testing at lower latitudes, Arctic testing will commence in the summer of 2026. DRDC will transport a sonobuoy simulator to their camp at Gascoyne Inlet to continue communication trials. When simulator testing is complete, sonobuoys will be deployed near the Gascoyne Inlet camp and in Lancaster Sound by ship. Support from the RCAF will be requested for Lancaster Sound deployments as required. If summer testing is deemed successful, additional testing during the fall and winter will be conducted with Geobuoys. The Geobuoys will be deployed in Lancaster Sound near the seasonal ice arch. This test plan will allow the functionality of the Audimus payload to be confirmed, prior to expending the significant resources required for an Arctic deployment and reducing the risk of failure. Upon completion of the initial ramp-up testing, Audimus will continue to collect data on an opportunity basis for the duration of its mission, including from other hydrophone systems.

### 7.2 Mission Operations

Audimus will operate in a polar orbit collecting acoustic data with a VHF receiver and downlinking the stored data to the RMC ground station via a UHF transmitter. Simulations of the Audimus orbit estimates approximately 14 passes over Lancaster Sound but only 6

over RMC daily necessitating a store and forward system for data management [113]. Average access times are 583s for the hydrophone and 540s for RMC. Given the 224 kbps data rate for the SSQ-573 sonobuoy, a maximum of 230 MB of data may be collected daily. The current ground station at RMC only offers a 9800 bps UHF downlink which is insufficient for the data collected. While the RMC ground station is being upgraded to allow for a greater volume to be downloaded, if collection from the primary sources is continuous, some data will still be lost.

An operations plan will be required to mitigate the potential effects of ionospheric disruptions. The planned hydrophone deployment location is near the auroral region which is subject to large scintillation effects along with auroral and polar cap absorption. Due to the limited margin highlighted in the link budget, these effects will likely prevent collection of acoustic data when they are present. Since these effects are driven by increased solar activity, which can be observed and predicted, they can be mitigated [47]. Deployment of sonobuoys can be controlled and avoided during periods of increased solar activity. Data collection can be delayed as these ionospheric events are generally short lived, 30 minutes to several hours [91]. Solar activity might disrupt one or two data collection attempts but should pass after a few orbits of Audimus which will be approximately 90 minutes. Regardless of mitigation measures, since Audimus will be launching during a period of heightened solar activity, some data loss will likely occur. This is acceptable however, since Audimus is a technology demonstrator and if some acoustic data is transferred the mission will be a success.

### **7.3 Mission Continuation**

If additional sources of acoustic data become available and quality data is being received by RMC, an extension of the Audimus mission could continue beyond its initial one-year period to capture the additional data sources. If the feasibility of a data uplink between Arctic hydrophones and Audimus is proven, a follow-on mission is recommended. The initial proposal for Audimus called for a low earth orbit (LEO) data relay to achieve near real-time reception of data (Figure 7.1). The in-orbit relay component was eventually deemed too risky for an initial technology demonstration mission and Audimus adopted a store-and-forward architecture for data management.

A successful mission in this configuration should lead to a follow-on mission with improved capabilities like the LEO data relay. This will bring the proof of concept in line with the original proposal of a constellation providing near-real time data which used paired satellite planes for data crosslink (Figure 7.2).

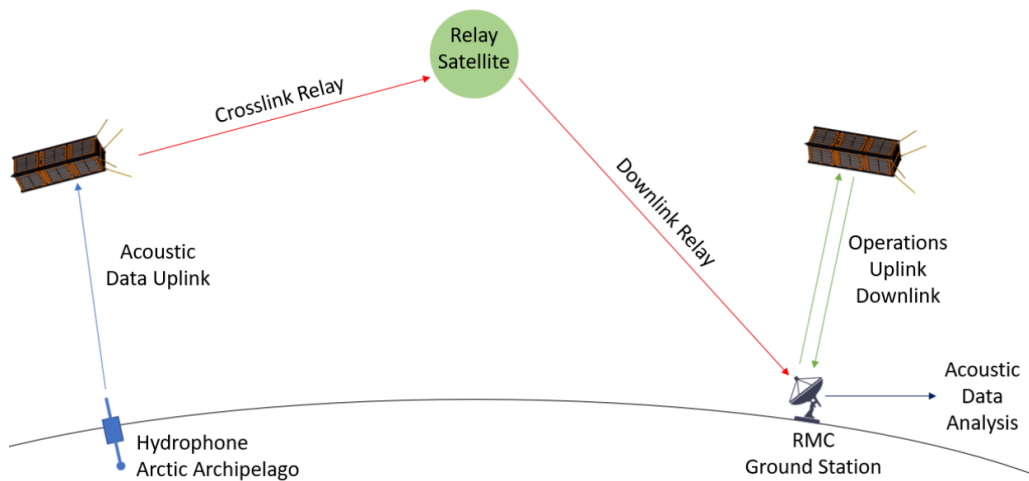


Figure 7.1 Initial Audimus Concept of Operations [21].

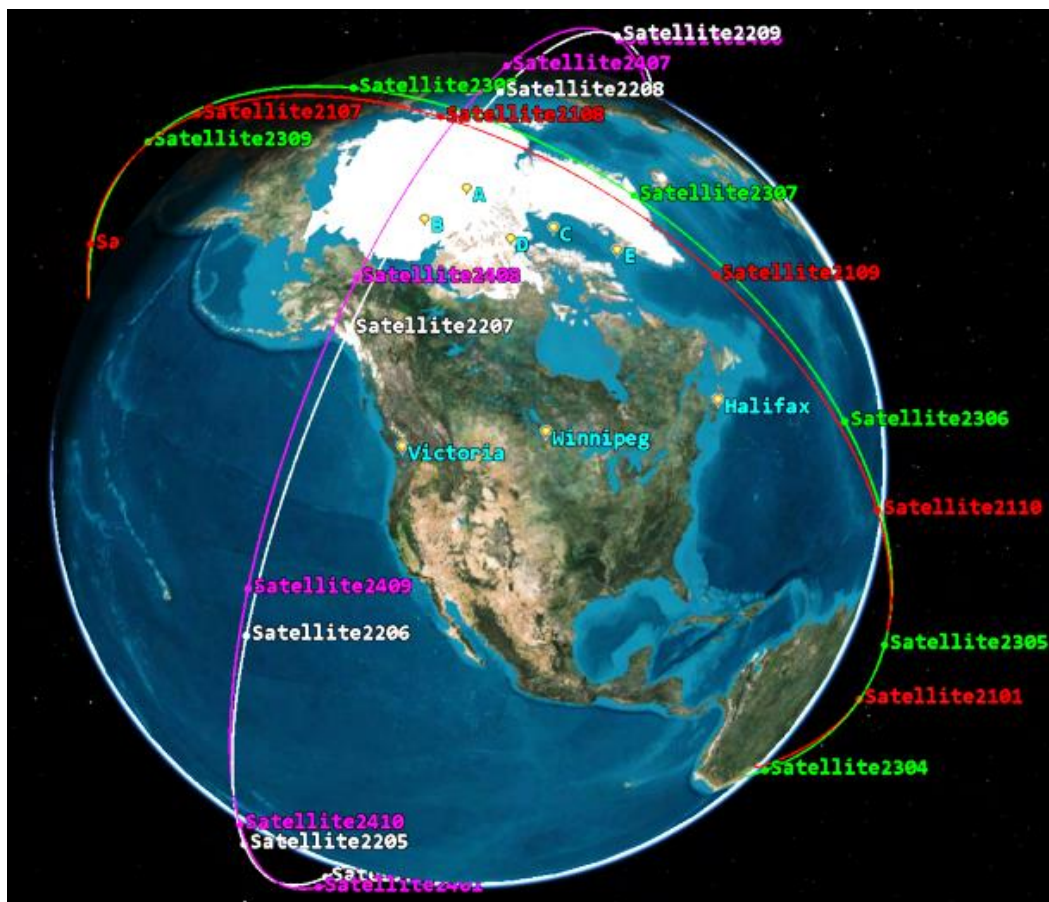


Figure 7.2 STK simulation of the proposed Walker Delta constellation with paired satellite planes. Strategic areas and potential ground stations are also indicated [22].

Continued development of SDR for CubeSats offers potential for a multi-mission system for Arctic surveillance. A single SDR can execute multiple applications simultaneously and could provide automatic dependent surveillance-broadcast (ADS-B) and automatic identification system (AIS) tracking in addition to acoustic data collection and high data rate communication further increasing domain awareness [124], [125]. Multiple applications will necessitate additional antennas, however antenna space on CubeSats is limited and will necessitate research into novel antenna design [126]. Additional areas for future work include continued development of Arctic hydrophone systems to provide continued coverage over a wider area along with year-round coverage.

## 8 Conclusion

The significant impact of global climate change on the Arctic is well established with the sea ice extent in the Arctic declining by more than 50% since consistent satellite observations of the region began in 1979. This has a profound effect on ice dynamics, weather patterns, and wildlife in the Arctic ecosystem. With a more accessible Arctic comes increasing ship traffic and military interest, particularly through the Northwest Passage presenting a challenge to Canada's sovereignty. Canada's monitoring capabilities are not sufficient to provide adequate situational awareness necessitating the need for greater investment and innovation. Improvements in small satellite technology offers additional opportunities for increased domain awareness.

The Audimus mission seeks to demonstrate the feasibility of transmitting acoustic data from a hydrophone in the Arctic to a LEO CubeSat. With data sources strategically placed in the Northwest Passage the acoustic information collected by Audimus can be used to monitor both marine vessel traffic while also providing oceanic data for the study ice dynamics and sea life. Lancaster Sound is one such strategic and ecologically important location in the Canadian Arctic Archipelago. The deployment of sonobuoys and subsequent data collection will offer insights to the acoustic environment of Lancaster Sound and the Northwest Passage, facilitating a deeper understanding of underwater acoustics in these strategic regions. A high-altitude balloon mission was used in validating system design, demonstrating the feasibility of the Audimus concept under real-world conditions. This demonstrator used traditional analog radios but the development of SDRs for CubeSats offers flexible, space proven solutions for the Audimus mission.

Effective ground-to-satellite communication is central to the success of the Audimus mission. A detailed analysis of the satellite communication link demonstrated that despite the weak RF signal from a sonobuoy, communication is possible within a small margin. The Arctic environment, however, presents unique challenges for RF communication, with increased ionospheric effects including scintillation, auroral and polar cap absorption. These effects will negatively impact communications, and because Audimus is launching during a period of heightened solar activity, will be unavoidable. An additional margin is needed in the link budget to combat these effects but is unavailable due to the communication link architecture and will need to be mitigated operationally instead. Some loss of data is acceptable since Audimus is a technology demonstrator. Only a small amount of acoustic data needs to be collected and relayed for the Audimus mission to be a success.

A successful Audimus mission will offer a scalable and adaptable framework for environmental monitoring and strategic operations in the Arctic. The lessons learned and the technological advancements realized through this mission provide a roadmap for future endeavors, reinforcing Canada's commitment to maintaining sovereignty and environmental stewardship in the rapidly changing Arctic region. Future work should focus on the continued development and deployment of addition Arctic hydrophone

systems to achieve year-round coverage over a broader area. The incorporation of a LEO data relay will align the mission capabilities with the original proposal of near-real-time data reception and allow persistent coverage.

## Bibliography

- [1] J. E. Box *et al.*, “Key Indicators of Arctic Climate Change: 1971–2017,” *Environ. Res. Lett.*, vol. 14, no. 4, p. 045010, Apr. 2019, doi: 10.1088/1748-9326/aafc1b.
- [2] C. B. Field and V. R. Barros, *Climate change 2014: impacts, adaptation, and vulnerability Working Group II contribution to the fifth assessment report of the Intergovernmental panel on climate change*. New York: Cambridge university press, 2014.
- [3] A. Kumar *et al.*, “Contribution of Sea Ice loss to Arctic Amplification,” *Geophysical Research Letters*, vol. 37, no. 21, 2010, doi: 10.1029/2010GL045022.
- [4] “The Sun sets on the Arctic melt season | Arctic Sea Ice News and Analysis.” Accessed: Apr. 05, 2024. [Online]. Available: <https://nsidc.org/arcticseaicenews/2023/10/the-sun-sets-on-the-arctic-melt-season/>
- [5] J. Dawson, L. Pizzolato, S. E. L. Howell, L. Copland, and M. E. Johnston, “Temporal and Spatial Patterns of Ship Traffic in the Canadian Arctic from 1990 to 2015,” *Arctic*, vol. 71, no. 1, pp. 15–26, 2018.
- [6] L. Pizzolato, S. E. L. Howell, J. Dawson, F. Laliberté, and L. Copland, “The Influence of Declining Sea Ice on Shipping Activity in the Canadian Arctic,” *Geophysical Research Letters*, vol. 43, no. 23, p. 12,146-12,154, 2016, doi: 10.1002/2016GL071489.
- [7] National Defence, “Our North, Strong and Free: A Renewed Vision for Canada’s Defence.” Accessed: Apr. 08, 2024. [Online]. Available: <https://www.canada.ca/en/department-national-defence/corporate/reports-publications/north-strong-free-2024.html>
- [8] Government of Canada, “Arctic and Northern Policy Framework.” Accessed: Apr. 08, 2024. [Online]. Available: <https://www.rcaanc-cirnac.gc.ca/eng/1560523306861/1560523330587>
- [9] “Northwest Passage | Definition, Explorers, Map, & Facts | Britannica.” Accessed: Jan. 24, 2024. [Online]. Available: <https://www.britannica.com/place/Northwest-Passage-trade-route>
- [10] R. Churchill, V. Lowe, and A. Sander, *The Law of the Sea*, Fourth. Manchester University Press, 2022.
- [11] R. Huebert, “Canadian Arctic Sovereignty and Security in a Transforming Circumpolar World,” in *Canada and the Changing Arctic*, F. Griffiths, R. Huebert, and P. W. Lackenbauer, Eds., Wilfrid Laurier Press, 2011, pp. 13–66. doi: 10.51644/9781554584130-008.
- [12] Senate of Canada, “Arctic Security Under Threat: Urgent needs in a changing geopolitical and environmental landscape,” SenCanada. Accessed: Apr. 23, 2024. [Online]. Available: <https://sencanada.ca/en/info-page/parl-44-1/secd-arctic-defence/>
- [13] “Arctic Security – CAF Operations and Exercises.” Accessed: Apr. 24, 2024. [Online]. Available: <https://www.canada.ca/en/department-national-defence/corporate/reports-publications/proactive-disclosure/secd-april-24-2023/arctic-security.html>
- [14] H. J. McKay, “A Secure and Sovereign Arctic,” Report of the Standing Committee on National Defence, 2023.
- [15] National Defence, “Challenge and Commitment: A Defence Policy for Canada.” Accessed: Apr. 24, 2024. [Online]. Available: <https://publications.gc.ca/site/eng/429765/publication.html>
- [16] “Harry DeWolf class.” Accessed: Apr. 24, 2024. [Online]. Available: <https://www.canada.ca/en/navy/corporate/fleet-units/surface/harry-dewolf-class.html>
- [17] “Royal Canadian Navy to Commission HMCS Harry DeWolf,” Overt Defense. Accessed: Apr. 24, 2024. [Online]. Available: <https://www.overtdefense.com/2021/06/24/royal-canadian-navy-to-commission-hmcs-harry-dewolf/>

- [18] Canadian Space Agency, “Earth Observation Satellites,” Canadian Space Agency. Accessed: Apr. 24, 2024. [Online]. Available: <https://www.asc-csa.gc.ca/eng/satellites/earth-observation/>
- [19] C. Richards, M. Pittman, K. Phelan, S. Nudds, and J. Hamilton, “The Barrow Strait Real Time Observatory: Under-ice Monitoring in the Canadian High Arctic,” Nov. 2017, pp. 1–7. doi: 10.1145/3148675.3152195.
- [20] “DFO’s Real-Time Arctic Ocean Observatory.” Accessed: Jan. 22, 2024. [Online]. Available: <https://www.bio.gc.ca/science/newtech-technouvelles/observatory-observatoire-en.php>
- [21] R. Vincent, “Proposal for Canadian Space Agency (CSA) CubeSats Initiative in Canada for STEM (CUBICS) 2022.” 2022.
- [22] S. C. Tarla, “A Satellite-Augmented Acoustic Surveillance System for the Canadian Arctic,” May 2023, Accessed: Jan. 24, 2024. [Online]. Available: <https://espace.rmc.ca:8443/jspui/handle/11264/1226>
- [23] “Ansys STK | Digital Mission Engineering Software.” Accessed: Jun. 05, 2024. [Online]. Available: <https://www.ansys.com/products/missions/ansys-stk>
- [24] P. C. Hines *et al.*, “Acoustic Propagation and Array Geometry for Strategic Arctic Areas,” JASCO Applied Sciences, Tech Report, 2023.
- [25] P. C. Hines *et al.*, “Arctic Acoustic Propagation Projections to 2040,” JASCO Applied Sciences, Technical Report, 2024.
- [26] W. D. Halliday *et al.*, “Vessel Risks to Marine Wildlife in the Tallurutiup Imanga National Marine Conservation Area and the Eastern Entrance to the Northwest Passage,” *Environmental Science & Policy*, vol. 127, pp. 181–195, Jan. 2022, doi: 10.1016/j.envsci.2021.10.026.
- [27] “Life and death in Lancaster Sound.” Accessed: Apr. 26, 2023. [Online]. Available: <https://canadiangeographic.ca/articles/life-and-death-in-lancaster-sound/>
- [28] Canada, “The North.” Accessed: Jun. 05, 2024. [Online]. Available: <https://natural-resources.canada.ca/earth-sciences/geography/atlas-canada/explore-our-maps/selected-thematic-maps/the-north/16886>
- [29] “Lancaster Sound,” Lancaster Sound. Accessed: Jun. 05, 2024. [Online]. Available: <http://lancastersound.wwf.ca>
- [30] K. L. Laidre *et al.*, “Arctic Marine Mammal Population Status, Sea Ice Habitat loss, and Conservation Recommendations for the 21st Century,” *Conservation Biology*, vol. 29, no. 3, pp. 724–737, 2015, doi: 10.1111/cobi.12474.
- [31] Parks Canada, “Inuit Impact and Benefit Agreement - Tallurutiup Imanga National Marine Conservation Area Inuit Impact and Benefit Agreement.” Accessed: Apr. 02, 2024. [Online]. Available: [https://parks.canada.ca/amnc-nmca/cnamnc-cnmca/~/\\_link.aspx?\\_id=30C68EC53D2A4B7C809E15130AD01DE3&\\_z=z](https://parks.canada.ca/amnc-nmca/cnamnc-cnmca/~/_link.aspx?_id=30C68EC53D2A4B7C809E15130AD01DE3&_z=z)
- [32] E. and C. C. Canada, “Historical Data - Climate - Environment and Climate Change Canada.” Accessed: Apr. 27, 2023. [Online]. Available: [https://climate.weather.gc.ca/historical\\_data/search\\_historic\\_data\\_e.html](https://climate.weather.gc.ca/historical_data/search_historic_data_e.html)
- [33] “The Science of Arctic Weather and Climate,” National Snow and Ice Data Center. Accessed: Jun. 06, 2024. [Online]. Available: <https://nsidc.org/learn/parts-cryosphere/arctic-weather-and-climate/science-arctic-weather-and-climate>
- [34] A. J. Pieńkowski, J. H. England, M. F. A. Furze, B. MacLean, and S. Blasco, “The late Quaternary Environmental Evolution of Marine Arctic Canada: Barrow Strait to Lancaster Sound,” *Quaternary Science Reviews*, vol. 91, pp. 184–203, May 2014, doi: 10.1016/j.quascirev.2013.09.025.

- [35] B. G. Sanderson and P. H. LeBlond, “The CrossChannel Flow at the Entrance of Lancaster Sound,” *Atmosphere-Ocean*, vol. 22, no. 4, pp. 484–497, Dec. 1984, doi: 10.1080/07055900.1984.9649211.
- [36] P. H. LeBlond, “On the Surface Circulation in Some Channels of the Canadian Arctic Archipelago,” *Arctic*, vol. 33, no. 1, pp. 189–197, 1980.
- [37] S. J. Prinsenberg and J. Hamilton, “Monitoring the Volume, Freshwater and Heat Fluxes Passing Through Lancaster Sound in the Canadian Arctic Archipelago,” *Atmosphere-Ocean*, vol. 43, no. 1, pp. 1–22, Mar. 2005, doi: 10.3137/ao.430101.
- [38] K. Jones-Williams, T. S. Galloway, V. L. Peck, and C. Manno, “Remote, but Not Isolated—Microplastics in the Sub-surface Waters of the Canadian Arctic Archipelago,” *Front. Mar. Sci.*, vol. 8, Jun. 2021, doi: 10.3389/fmars.2021.666482.
- [39] T. Yao and C. L. Tang, “The formation and maintenance of the North Water Polynya,” *Atmosphere-Ocean*, vol. 41, no. 3, pp. 187–201, Sep. 2003, doi: 10.3137/ao.410301.
- [40] R. Vincent, “An Assessment of the Lancaster Sound Polynya Using Satellite Data 1979 to 2022,” *Remote Sensing*, 2023.
- [41] “NOAA’s Comprehensive Large Array-data Stewardship System.” Accessed: Apr. 26, 2023. [Online]. Available: [https://www.avl.class.noaa.gov/saa/products/search?sub\\_id=0&datatype\\_family=AVHRR&submit.x=24&submit.y=4](https://www.avl.class.noaa.gov/saa/products/search?sub_id=0&datatype_family=AVHRR&submit.x=24&submit.y=4)
- [42] N. C. for E. Information (NCEI), “Earth’s Magnetic Field Calculators - Instructions | NCEI.” Accessed: Jun. 06, 2024. [Online]. Available: <https://www.ngdc.noaa.gov/geomag/magfield.shtml>
- [43] “Predicted Sunspot Number And Radio Flux | NOAA / NWS Space Weather Prediction Center.” Accessed: Jun. 06, 2024. [Online]. Available: <https://www.swpc.noaa.gov/products/predicted-sunspot-number-and-radio-flux>
- [44] “World Magnetic Model (WMM),” National Centers for Environmental Information (NCEI). Accessed: May 25, 2024. [Online]. Available: <https://www.ncei.noaa.gov/products/world-magnetic-model>
- [45] “Solar Cycle Progression | NOAA / NWS Space Weather Prediction Center.” Accessed: Feb. 28, 2024. [Online]. Available: <https://www.swpc.noaa.gov/products/solar-cycle-progression>
- [46] Natural Resources Canada, “Space Weather Canada.” Accessed: Oct. 30, 2024. [Online]. Available: <https://www.spaceweather.gc.ca/index-en.php>
- [47] “NOAA / NWS Space Weather Prediction Center.” Accessed: Oct. 31, 2024. [Online]. Available: <https://www.swpc.noaa.gov/communities/aurora-dashboard-experimental>
- [48] “Canadian High Arctic Ionospheric Network.” Accessed: Jun. 06, 2024. [Online]. Available: <http://chain.physics.unb.ca/chain/pages/about/>
- [49] H. Villeneuve and T. Thayaparan, “Canadian High Arctic Ionospheric Models (CHAIM),” Defence Research and Development Canada, 2021.
- [50] B. Larson, A. V. Koustov, D. R. Themens, and R. G. Gillies, “Ionospheric Electron Density Over Resolute Bay According to E-CHAIM Model and RISR Radar Measurements,” *Advances in Space Research*, vol. 71, no. 6, pp. 2759–2769, Mar. 2023, doi: 10.1016/j.asr.2023.01.017.
- [51] L. M. Brekhovskikh and Yu. P. Lysanov, *Fundamentals of Ocean Acoustics*. in Modern Acoustics and Signal Processing. New York: Springer-Verlag, 2003. doi: 10.1007/b97388.
- [52] P. C. Etter, *Underwater Acoustic Modeling and Simulation*, 5th ed. 2018. Accessed: Jun. 13, 2024. [Online]. Available: <https://www.routledge.com/Underwater-Acoustic-Modeling-and-Simulation/Etter/p/book/9781138054929>

- [53]H. Medwin, “Speed of Sound in Water: A Simple Equation for Realistic Parameters,” *The Journal of the Acoustical Society of America*, vol. 58, no. 6, pp. 1318–1319, Dec. 1975, doi: 10.1121/1.380790.
- [54]J. Shibley, “Enhanced Sonar Array Target Localization Using Time-Frequency Interference Phenomena,” *Dissertations and Theses*, Dec. 2013, doi: 10.15760/etd.1487.
- [55]H. Medwin and C. S. Clay, *Fundamentals of Acoustical Oceanography*. in Applications of modern acoustics. Boston: Academic Press, 1998.
- [56]N. Simão, “Seismicity of the Mid-Atlantic Ridge in the MoMAR area at a regional scale, observed by autonomous hydrophone arrays,” Nov. 2009.
- [57]M. K. Prior, O. Meless, P. Bittner, and H. Sugioka, “Long-Range Detection and Location of Shallow Underwater Explosions Using Deep-Sound-Channel Hydrophones,” *IEEE Journal of Oceanic Engineering*, vol. 36, no. 4, pp. 703–715, Oct. 2011, doi: 10.1109/JOE.2011.2154390.
- [58]R. Xue, Y. Yang, J. Weng, H. Wen, H. Chen, and L. Lin, “Modelling Convergence Zone Propagation Under the Influence of Arctic Front,” in *2021 OES China Ocean Acoustics (COA)*, Jul. 2021, pp. 229–233. doi: 10.1109/COA50123.2021.9520075.
- [59]“Sonar Propagation.” Accessed: Jun. 21, 2024. [Online]. Available: [https://man.fas.org/dod-101/navy/docs/es310/SNR\\_PROP/snr\\_prop.htm](https://man.fas.org/dod-101/navy/docs/es310/SNR_PROP/snr_prop.htm)
- [60]E. Giesbrecht, “Acoustic Modelling to Inform Policies: Mitigating Vessel Noise Impacts on Arctic Cetaceans Within the Tallurutiup Imanga National Marine Conservation Area,” Report, Nov. 2018. Accessed: Jun. 20, 2024. [Online]. Available: <https://DalSpace.library.dal.ca//handle/10222/75166>
- [61]P. Alexander, A. Duncan, N. Bose, and D. Smith, “Modelling Acoustic Transmission Loss Due to Sea Ice Cover.,” *Acoustics Australia*, vol. 41, no. 1, pp. 79–87, Apr. 2013.
- [62]S. Li, S. Yuan, S. Liu, J. Wen, Q. Huang, and Z. Zhang, “Characteristics of Low-Frequency Acoustic Wave Propagation in Ice-Covered Shallow Water Environment,” *Applied Sciences*, vol. 11, p. 7815, Aug. 2021, doi: 10.3390/app11177815.
- [63]P. F. Worcester, “Ocean Acoustics in the Rapidly Changing Arctic,” *Acoust. Today*, vol. 16, no. 1, p. 55, 2020, doi: 10.1121/AT.2020.16.1.55.
- [64]D. L. Barrett, “Lancaster Sound Shipborne Magnetometer Survey,” *Canadian Journal of Earth Sciences*, Feb. 2011, doi: 10.1139/e66-018.
- [65]B. MacLean *et al.*, “Seafloor features delineate Late Wisconsinan ice stream configurations in eastern Parry Channel, Canadian Arctic Archipelago,” *Quaternary Science Reviews*, vol. 160, pp. 67–84, Mar. 2017, doi: 10.1016/j.quascirev.2017.02.001.
- [66]W. D. Halliday *et al.*, “Underwater sound levels in the Canadian Arctic, 2014–2019,” *Marine Pollution Bulletin*, vol. 168, p. 112437, Jul. 2021, doi: 10.1016/j.marpolbul.2021.112437.
- [67]E. Cook, D. Barclay, and C. Richards, “Ambient Noise in the Canadian Arctic,” in *Governance of Arctic Shipping*, Springer, Cham, 2020, pp. 105–133. doi: 10.1007/978-3-030-44975-9\_6.
- [68]E. Jansen and C. de Jong, “Experimental Assessment of Underwater Acoustic Source Levels of Different Ship Types,” *IEEE Journal of Oceanic Engineering*, vol. 42, no. 2, pp. 439–448, Apr. 2017, doi: 10.1109/JOE.2016.2644123.
- [69]S. Merz, R. Kinns, and N. Kessissoglou, “Structural and acoustic responses of a submarine hull due to propeller forces,” *Journal of Sound and Vibration*, vol. 325, no. 1, pp. 266–286, Aug. 2009, doi: 10.1016/j.jsv.2009.03.011.
- [70]J. Hamilton, S. B. Martin, N. E. Chorney, A. J. Cole, and P. Borys, “Arctic Buoy Component Investigations,” JASCO Applied Sciences, Technical Report, 2023.

- [71]“Innovation, Science, and Economic Development Canada Proposal: LCC-VLA.” JASCO Applied Sciences, 2023.
- [72]“Defence & Security,” JASCO Applied Sciences. Accessed: Jul. 11, 2024. [Online]. Available: <https://www.jasco.com/defence>
- [73]“SIMB3 | Through-Ice Observation, 24-7/365.” Accessed: Jul. 11, 2024. [Online]. Available: <https://www.cryosphereinnovation.com/simb3>
- [74]“icListen HF,” Ocean Sonics. Accessed: Jan. 22, 2024. [Online]. Available: <https://oceansonics.com/products/iclisten-sj9/>
- [75]K. Iqbal, M. Zhang, S. Piao, and H. Ge, “Evolution of Sonobuoy through History & its Applications: A Survey,” in *2020 17th International Bhurban Conference on Applied Sciences and Technology (IBCAST)*, Jan. 2020, pp. 543–554. doi: 10.1109/IBCAST47879.2020.9044549.
- [76]“UAVs vs Subs,” Royal Aeronautical Society. Accessed: Jan. 22, 2024. [Online]. Available: <https://www.aerosociety.com/news/uavs-vs-subs/>
- [77]ULTRA Maritime, “AN/SSQ-53 Sonobuoy Datasheet.” ULTRA Maritime, 2021. Accessed: Apr. 02, 2023. [Online]. Available: [https://www.ultra.group/media/2448/anssq-53d3-datasheet\\_final.pdf](https://www.ultra.group/media/2448/anssq-53d3-datasheet_final.pdf)
- [78]“Sonobuoy AN/SSQ-53D(3) Transmitter - Measurement of Radiofrequency Characteristics.” QETE Test Report, 2021.
- [79]“MATLAB.” Accessed: Jul. 22, 2024. [Online]. Available: <https://www.mathworks.com/products/matlab.html>
- [80]ULTRA Maritime, “AN/SSQ-573 Sonobuoy Datasheet.” ULTRA Maritime, 2021. Accessed: Apr. 02, 2023. [Online]. Available: [https://www.ultra.group/media/2662/anssq-573-datasheet\\_final.pdf](https://www.ultra.group/media/2662/anssq-573-datasheet_final.pdf)
- [81]Defence Research and Development Canada, “Spring 2015 Geobuoy Comparison Trial.” Accessed: Jun. 13, 2024. [Online]. Available: <https://www.canada.ca/en/defence-research-development/news/articles/spring-2015-geobuoy-comparison-trial.html>
- [82]R. I. Verrall, G. J. Heard, and S. Blouin, “The History of Defence Science in the Canadian Arctic”.
- [83]“Arctic Submarine Warfare - NSL Archive.” Accessed: Jun. 14, 2024. [Online]. Available: <https://archive.navalsubleague.org/1989/arctic-submarine-warfare-2>
- [84]D. Mosher *et al.*, “High Arctic Marine Geophysical Data Acquisition,” *The Leading Edge*, vol. 32, pp. 524–536, May 2013, doi: 10.1190/tle32050524.1.
- [85]J. D. Jackson, *Classical Electrodynamics*, 3rd ed. Wiley, 1998.
- [86]D. J. Griffiths, *Introduction to Electrodynamics*. Cambridge University Press, 2017.
- [87]D. Roddy, *Satellite Communications*, 4th Edition. McGraw-Hill Education, 2006.
- [88]P. Rohan, *Introduction to Electromagnetic Wave Propagation*. Boston: Artech House, 1991.
- [89]L. Ippolito, *Propagation Effects Handbook for Satellite Systems Design - Section 1 Background*, 5th ed. Stanford Telecom, 1999.
- [90]T. Pratt and J. Allnut, *Satellite Communications*, 3rd ed. Wiley, 2020.
- [91]International Telecommunication Union, “Recommendation ITU-R P.531-15 (08/2023) - Ionospheric propagation data and prediction methods required for the design of satellite networks and systems.” Accessed: Oct. 31, 2024. [Online]. Available: <https://www.itu.int/rec/R-REC-P.531/en>
- [92]Y. Jiao, Y. T. Morton, S. Taylor, and W. Pelgrum, “Characterization of High-Latitude Ionospheric Scintillation of GPS Signals,” *Radio Science*, vol. 48, no. 6, pp. 698–708, 2013, doi: 10.1002/2013RS005259.

- [93] L. Ippolito, *Propagation Effects Handbook for Satellite Systems Design - Section 2 Prediction*, 5th ed. Stanford Telecom, 1999.
- [94] International Telecommunication Union, “Recommendation ITU-R P.618-14 (08/2023) - Propagation data and prediction methods required for the design.” Accessed: Oct. 31, 2024. [Online]. Available: <https://www.itu.int/rec/R-REC-P.531-15-202308-I/en>
- [95] J. Wertz, D. Everett, and J. Puschell, *Space Mission Engineering: The New SMAD*. Microcosm Press, 2011.
- [96] “Antenna Theory and Design, 3rd Edition | Wiley,” Wiley.com. Accessed: Jul. 05, 2024. [Online]. Available: <https://www.wiley.com/en-us/Antenna+Theory+and+Design%2C+3rd+Edition-p-9780470576649>
- [97] “Earth Fact Sheet.” Accessed: Jul. 05, 2024. [Online]. Available: <https://nssdc.gsfc.nasa.gov/planetary/factsheet/earthfact.html>
- [98] E. Udnæs, “Antenna Design for UHF Satellite Communication from Sensor Nodes in the Arctic,” Master thesis, NTNU, 2019. Accessed: May 25, 2024. [Online]. Available: <https://ntnuopen.ntnu.no/ntnu-xmlui/handle/11250/2624673>
- [99] “CSA CUBICS Webinar 013 - Telecommunications,” Accessed: Oct. 30, 2024. [Online]. Available: [https://docs.google.com/presentation/d/1Yd93wWMAEX1F3WPM\\_P\\_AdUVK2DfxVjO0](https://docs.google.com/presentation/d/1Yd93wWMAEX1F3WPM_P_AdUVK2DfxVjO0)
- [100] I. Savytsky, “Personal Communication,” Jan. 2024.
- [101] D. Vallado, *Fundamentals of Astrodynamics and Applications*, 5th ed. Accessed: Oct. 31, 2024. [Online]. Available: <http://astrobooks.com/vallado5hb.aspx>
- [102] B. H. Maranda, “Calibration Factors for DIFAR Processing,” DRDC, Technical Memorandum, 2001. [Online]. Available: <https://cradpdf.drdc-rddc.gc.ca/PDFS/unc82/p518209.pdf>
- [103] A. Fanfani, S. Morosi, L. S. Ronga, and E. Del Re, “Effective Doppler Mitigation in Critical Satellite Communications,” in *Wireless and Satellite Systems*, I. Otung, P. Pillai, G. Eleftherakis, and G. Giambene, Eds., Cham: Springer International Publishing, 2017, pp. 145–155. doi: 10.1007/978-3-319-53850-1\_15.
- [104] “International Space Mission Training -CREATE Your Future – An NSERC Funded CREATE Training Program.” Accessed: Mar. 08, 2024. [Online]. Available: <http://spacemissiontraining.ca/>
- [105] “BaoFeng UV-5R,” BaoFeng Radios. Accessed: Jun. 14, 2024. [Online]. Available: <https://baofengtech.com/product/uv-5r/>
- [106] “4nec2 antenna modeler and optimizer.” Accessed: Jul. 04, 2024. [Online]. Available: <https://www.qsl.net/4nec2/>
- [107] “Audacity ® | Free Audio editor, recorder, music making and more!” Accessed: Apr. 07, 2024. [Online]. Available: <https://www.audacityteam.org/>
- [108] “WiNRADiO WR-G39WSBe Sonobuoy Telemetry Receiver.” Accessed: Jul. 13, 2024. [Online]. Available: <https://winradio.com/home/g39wsbe.htm>
- [109] S. Rankin, B. Miller, J. L. Crance, T. Sakai, and J. L. Keating, “Sonobuoy Acoustic Data Collection during Cetacean Surveys”, Accessed: Jul. 13, 2024. [Online]. Available: <https://repository.library.noaa.gov/view/noaa/20265>
- [110] B. Miller *et al.*, “Accuracy and precision of DIFAR localisation systems: Calibrations and comparative measurements from three SORP voyages,” May 2014.
- [111] A. Kuzu *et al.*, “Laboratory and Sea Testing of DIFAR Sonobuoys,” in *2012 IV International Congress on Ultra Modern Telecommunications and Control Systems*, Oct. 2012, pp. 385–390. doi: 10.1109/ICUMT.2012.6459697.

- [112] “Sonobuoy Receivers,” Ultra Maritime. Accessed: Nov. 01, 2024. [Online]. Available: <https://umaritime.com/sonobuoy-receivers/>
- [113] “Audimus Preliminary Design Review Document for CSA,” RMC, 2024.
- [114] Cal Poly, “CubeSat Design Specification.” Cal Poly, Feb. 2022. Accessed: Apr. 13, 2023. [Online]. Available: [https://static1.squarespace.com/static/5418c831e4b0fa4ecac1bacd/t/62193b7fc9e72e0053f00910/1645820809779/CDS+REV14\\_1+2022-02-09.pdf](https://static1.squarespace.com/static/5418c831e4b0fa4ecac1bacd/t/62193b7fc9e72e0053f00910/1645820809779/CDS+REV14_1+2022-02-09.pdf)
- [115] “CubeSat.Market,” Cubesat Market. Accessed: Jul. 13, 2024. [Online]. Available: <https://www.cubesat.market>
- [116] “CubeSatShop.com - One-stop webshop for CubeSats & Nanosats.” Accessed: Jul. 13, 2024. [Online]. Available: <https://www.cubesatshop.com/>
- [117] SatCatalog, “Home | SatCatalog.” Accessed: Jul. 13, 2024. [Online]. Available: <https://www.satcatalog.com/>
- [118] “9.0 Communications - NASA.” Accessed: Jul. 13, 2024. [Online]. Available: <https://www.nasa.gov/smallsat-institute/sst-soa/soa-communications/>
- [119] “Pulsar-VUTRX - CubeSat VHF/UHF Transceiver | AAC Clyde Space.” Accessed: Jul. 13, 2024. [Online]. Available: <https://www.aac-clyde.space/what-we-do/space-products-components/communications/pulsar-vutrx>
- [120] B. KHOUANE, N. Belbekri, and J. E. Benmansour, “An Overview of Software-Defined Radio Technology in CubeSat Communications,” *Algerian Journal of Signals and Systems*, vol. 8, pp. 55–58, Dec. 2023, doi: 10.51485/ajss.v8i2.189.
- [121] “TOTEM: Software Defined Radio,” Alén Space. Accessed: Jul. 13, 2024. [Online]. Available: <https://alen.space/products/totem-sdr/>
- [122] “CubeSat Antenna System for 1U/3U,” ISISPACE. Accessed: Jul. 13, 2024. [Online]. Available: <https://www.isispace.nl/product/cubesat-antenna-system-1u-3u/>
- [123] “GNU Radio.” Accessed: Jul. 12, 2024. [Online]. Available: <https://www.gnuradio.org/>
- [124] R. Vincent and R. V. D. Pryt, “The CanX-7 Nanosatellite ADS-B Mission: A Preliminary Assessment,” *Positioning*, vol. 8, no. 1, Art. no. 1, Feb. 2017, doi: 10.4236/pos.2017.81001.
- [125] “TREVO: Modular High Performance SDR Platform,” Alén Space. Accessed: Jul. 13, 2024. [Online]. Available: <https://alen.space/products/trevo/>
- [126] J. Huang, Z. Hussein, and A. Petros, “A Wide-Band Dual-Polarized VHF Microstrip Antenna for Global Sensing of Sea Ice Thickness,” in *2005 IEEE Antennas and Propagation Society International Symposium*, Jul. 2005, pp. 684–687 vol. 2B. doi: 10.1109/APS.2005.1552106.